ELSEVIER

Contents lists available at ScienceDirect

Applied Energy

journal homepage: www.elsevier.com/locate/apenergy



Bilevel optimization for multi-user systems with mixed demand response programs for enhanced operational efficiency in electric power grids

Young-Bin Woo^a, Ilkyeong Moon^{b,c,*}

- ^a Keio Frontier Research & Education Collaborative, Keio University, 7-7 Shinkawasaki, Saiwai Ward, Kawasaki, Kanagawa 212-0032, Japan
- ^b Department of Industrial Engineering, Seoul National University, 1 Gwanak-ro, Gwanak-gu, Seoul 08826, Republic of Korea
- c Institute for Engineering Research, Seoul National University, 1 Gwanak-ro, Gwanak-gu, Seoul 08826, Republic of Korea

HIGHLIGHTS

- A hierarchical interaction model between an system operator and users is formulated.
- A reformulation-and-decomposition algorithm is proposed to address bilevel feasibility,
- Two demand response program settings are compared through computational experiments.
- The applicability of the proposed solution approach is presented.
- Results reveal the economic and operational benefits of demand response participation.

ARTICLE INFO

Keywords: Bilevel programming Demand response Distributed energy resources Decentralized grid Peak load reduction

ABSTRACT

Decentralized power grid systems present new challenges for independent system operators (ISOs) in balancing electricity demand, ensuring grid stability, and optimizing operational costs. A bilevel optimization problem is introduced to represent the hierarchical decision-making process between an ISO and multiple electricity users. The ISO sets subsidy rates and real-time pricing (RTP) to influence user behavior while users optimize their energy consumption and distributed energy resource (DER) operations. A reformulation-and-decomposition algorithm is proposed to address bilevel feasibility issues and to improve computational efficiency. Computational experiments compare two demand response programs (DRPs) settings on subsidy programs and RTP. The results show that integrating RTP enhances bilevel feasibility, improves peak load reduction, and increases computational complexity. Budget allocation significantly impacts DRP effectiveness, with diminishing returns at higher levels. The findings highlight the benefits of a mixed DRP approach for improving decentralized grid operations.

1. Introduction

1.1. Background

Electricity consumption has rapidly increased globally over the last few decades. Globally, power grids are continuously evolving, transitioning from traditional static architectures to increasingly complex networks. This transformation highlights the necessity of innovative operational strategies that extend beyond the simple delivery of electricity to focus on efficiently managing energy resources and maintaining grid stability [1–3]. Peak load management is one of the core challenges in grid operations. When electricity demand exceeds the grid's capacity, it can result in transmission network overloads, outages,

and other critical issues. Developing effective strategies to reduce peak loads and ensure grid stability is thus essential. The California duck curve is a representative example of such challenges. In California, the growing share of renewable energy sources, such as solar power, has sharply decreased electricity demand during daylight hours. However, as solar generation ceases in the evening, electricity demand spikes significantly, resulting in wider operational fluctuations for the grid. This phenomenon illustrates the unintended consequences of renewable energy expansion and the new challenges to maintaining grid stability. Consequently, modern research emphasizes the need for diversified strategies that optimize grid operations, even if distributed energy resources (DERs) are not exclusively based on renewable sources [4]. Adopting this perspective, this study models interactions between ISOs

^{*} Corresponding author at: Department of Industrial Engineering, Seoul National University, 1 Gwanak-ro, Gwanak-gu, Seoul 08826, Republic of Korea. E-mail addresses: ybwoo@keio.jp (Y.-B. Woo), ikmoon@snu.ac.kr (I. Moon).

and multiple electricity users to propose methodologies aimed at simultaneously reducing peak loads and enhancing grid stability.

An independent system operator (ISO) plays a pivotal role in grid operations by ensuring grid stability and facilitating the efficient flow of electricity. ISOs manage electricity transmission, coordinate market transactions, and implement measures to maintain physical grid stability. Key responsibilities include balancing power flows between generators and consumers, managing grid bottlenecks, and implementing recovery plans during emergencies. On the other hand, electricity users are integral components of the grid, consuming or generating electricity. They can evolve beyond mere consumers into prosumers who produce and sell surplus power. Some electricity users may transition into potential microgrids, forming self-sufficient energy systems that contribute to regional energy independence. Among these roles, ISOs use mechanisms such as real-time pricing (RTP) and subsidy policies to guide user behavior and maximize grid efficiency.

Modern electricity markets are categorized into various structures based on trading mechanisms and energy management models. This study highlights the significance of regional, decentralized electricity markets, where multiple microgrids and prosumers aim for regional energy independence and efficient DER utilization. In these markets, individual microgrids and prosumers develop autonomous production and consumption strategies, while ISOs coordinate their interactions to ensure optimal distribution of local energy resources and to maintain grid stability. This study proposes strategies to efficiently facilitate DER installation and operation in such markets. Leveraging RTP, dynamic pricing policies, and subsidy frameworks provides actionable insights into influencing user behavior and promoting DER adoption.

Discussions on related issues are abundant in the literature [5–8]. Topics such as ISO-user interactions, the effectiveness of demand response programs, optimal DER placement and operation, and the application of bilevel optimization in hierarchical decision-making structures are particularly prevalent. These discussions form a significant theoretical and practical foundation for simultaneously addressing grid stability and economic considerations. Details are elaborated in the subsequent subsection.

1.2. Literature review

Recent advancements in energy management and multi-microgrid systems highlight the critical role of bilevel optimization, demand response programs, DERs, and ISO-user interactions. These studies aim to address the complexities of modern power systems, integrating technical innovations with economic and environmental considerations. This section provides an overview of key contributions categorized by their primary focus.

Bilevel optimization methodologies have been extensively applied to address hierarchical decision-making in energy systems. These methodologies provide solutions for complex energy management problems, enabling effective coordination between different stakeholders. For instance, Bahramara et al. [9] introduced a hierarchical framework for active distribution grids, enabling value-based pricing of distributed resources. Marvasti et al. [10] proposed a system-of-systems approach for active distribution grids, leveraging bilevel optimization for economic dispatch. Similarly, Rider et al. [11] developed a mixed-integer linear programming model for optimal pricing and location of distributed generation in radial distribution systems. Mobarakeh et al. [12] extended this concept to contract pricing of independent dispatchable distributed generator (DG) units, employing a bilevel pricing strategy. Liu et al. [13] presented a robust operation-based scheduling framework for smart distribution networks, incorporating multiple microgrids under uncertainty. Collectively, these studies demonstrate the flexibility and scalability of bilevel optimization for modern power grids but often overlook the practical implementation challenges in scenarios.

Demand response programs (DRPs) have emerged as a pivotal strategy for balancing grid operations and enhancing user participation.

These programs integrate dynamic pricing and load-shifting mechanisms to align user consumption with grid requirements. Georgia et al. [14] explored leader-follower strategies for energy management in multi-microgrids, combining cooperative and competitive trading mechanisms. Wang et al. [15] investigated hierarchical power scheduling for macrogrid and microgrid coordination, emphasizing multi-level power scheduling under DRPs. Hamid and Shahram [16] presented a stochastic multi-objective framework for optimal energy management in multi-microgrids, integrating DRPs with distributed energy resources. Li et al. [17] developed a distributed control method for high-penetration renewable energy in multi-microgrids, highlighting the synergy between DRPs and DER integration. While DRPs effectively balance supply and demand, their scalability and integration with renewable sources remain ongoing challenges in implementation.

DER integration, coupled with storage systems, has become a cornerstone of modern energy management. These systems enhance the resilience and sustainability of energy systems by leveraging renewable resources and energy storage technologies. Radhakrishnan and Srinivasan [18] proposed a multi-agent-based distributed energy management scheme, optimizing wind and solar generation in smart grids. Nikmehr and Ravadanegh [19] focused on optimal power dispatch in multi-microgrids, incorporating solar, wind, and biomass resources. Felipe and Tapas [20] developed a bilevel model for emissions reduction policies in carbon-priced markets, utilizing wind and biomass DERs. Han and Lee [21] introduced a two-stage stochastic programming model for multi-microgrid design and operation, emphasizing renewable energy sources. Hossein and Reza [22] presented novel technical indices for designing and operating multi-microgrid distribution networks, emphasizing their role in enhancing operational efficiency. However, the integration of DERs with grid-scale energy storage systems continues to face technical and economic barriers, particularly in terms of costeffectiveness and reliability.

ISO-user interactions form a critical component of energy management, particularly in decentralized and peer-to-peer energy markets. These interactions enable efficient coordination between grid operators and users, fostering collaborative energy management strategies. Gregoratti and Matamoros [23] modeled distributed energy trading for multi-microgrid scenarios, emphasizing decentralized market structures. Esther et al. [24] designed peer-to-peer energy markets within urban microgrids, demonstrating the feasibility of local energy transactions. Saad et al. [25] employed coalitional game theory to optimize microgrid distribution networks, fostering cooperative strategies among users. Wang et al. [26] proposed a peer-to-peer transaction method for diversified prosumers in urban microgrids, highlighting the potential of localized energy trading. While these studies illustrate the feasibility of decentralized energy systems, challenges remain in standardizing transaction protocols and in ensuring equitable resource allocation across participants.

Despite these contributions, existing studies often lack comprehensive frameworks for multi-follower decision-making in hierarchical structures. Many focus narrowly on single-layer optimization or specific DRP implementations, limiting their applicability to broader, real-world contexts. In contrast, the study presented in Section 3 addresses these limitations by developing a bilevel optimization model tailored for ISO-user interactions, incorporating multi-follower decision-making and RTP strategies, thereby bridging critical gaps in prior research.

1.3. Research gap and key contributions

While existing studies on demand response and DER coordination have offered foundational insights, they often focus on single-user scenarios or isolated microgrid systems, overlooking the complexity of multi-user interactions and hierarchical decision-making in realistic power systems. While these models offer analytical simplicity, they overlook the complexity of multi-user interactions and the hierarchical decision-making structure present in real-world power systems.

Additionally, the integration of RTP and installation subsidies has been explored separately, with limited attention given to their combined effects under budget constraints. Furthermore, many bilevel optimization approaches fail to scale efficiently when incorporating discrete user-level decisions.

To address these limitations, this study addresses the following core question: How can we design a bilevel demand response framework that effectively combines RTP and installation subsidies while maintaining computational scalability and behavioral realism in multi-user settings? To this end, a comprehensive framework is proposed to capture the operational, economic, and computational challenges involved in coordinating multiple electricity users under a unified demand response mechanism. The main contributions of this study are as follows: A bilevel optimization model is formulated to describe the hierarchical interaction between an ISO and multiple electricity users.

- A mixed-incentive scheme is introduced, combining RTP and budgetlimited subsidies to influence user participation and DER adoption.
- A scalable solution method is developed using reformulation based on Karush–Kuhn–Tucker (KKT) conditions and generalized Benders decomposition to address the resulting mixed-integer structure.
- Simulation experiments are conducted to evaluate the effects of the incentive mechanisms on both user behavior and grid-level outcomes.

These contributions collectively establish a modeling and algorithmic framework that bridges the gap between theoretical bilevel optimization and practical DR program design. In particular, the proposed solution method improves scalability by decoupling ISO-level and user-level decisions through a KKT-based reformulation, and efficiently handles discrete installation decisions using generalized Benders decomposition. This technical structure distinguishes it from conventional bilevel methods that typically rely on full enumeration or heuristic approximations. Moreover, the joint analysis of RTP and subsidy mechanisms allows for a more accurate reflection of real-world incentive environments, and the simulation results provide concrete guidance on policy design under realistic budget constraints.

To further clarify the novelty and practical advantages of the proposed approach, a comparison is provided with traditional bilevel optimization techniques used in related studies. Traditional approaches, particularly those based on single-level reformulations using KKT conditions or complementarity constraints, often result in large-scale nonconvex programs that face difficulties when incorporating discrete follower-level decisions. Such methods also suffer from infeasibility issues, especially under budget-constrained bilevel formulations where the leader's feasible region is not guaranteed to align with the follower's optimal response. In contrast, the proposed algorithm adopts a hybrid strategy that reformulates each follower's problem under fixed discrete decisions using KKT conditions and embeds these into a generalized Benders decomposition framework. This two-level design separates bestresponse computation from bilevel feasibility validation through distinct subproblems, thereby enabling robust convergence. Furthermore, by using special ordered set type 1 (SOS1) constraints, the algorithm avoids reliance on large big-M constants, thereby improving numerical stability and model interpretability. These structural enhancements make the proposed algorithm well-suited for realistic DRP design environments, where system-scale coordination, budget limitations, and combinatorial user behavior must be simultaneously addressed.

1.4. Paper organization

The remainder of the paper is organized as follows. Section 2 introduces the research problem, detailing the nature of ISO-user interactions and the role of demand response programs in improving grid operations. Section 3 describes the bilevel optimization framework,

presenting the mathematical formulations for ISO and user objectives. It also describes the development of a computational algorithm to solve the optimization problem efficiently in Section 4. Section 5 discusses the experimental design, the performance metrics, and the results, demonstrating the practical applicability and effectiveness of the framework. Finally, conclusions are drawn, and areas for future work are recommended in Section 5.

2. Problem description

2.1. Problem statement

The ISO serves as the central coordinator in the electricity grid, facilitating efficient energy flow and maintaining system stability. As depicted in Fig. 1, the ISO procures electricity from the main grid and distributes it to multiple electricity users (or microgrids). Through RTP and subsidy programs, the ISO balances its multi-objective framework by influencing electricity users to achieve grid stability and cost optimization goals. In the RTP program, the ISO predetermines real-time retail electricity prices, enabling followers to observe price signals and adjust their consumption patterns accordingly. Followers respond by shifting their electricity usage to periods where the ISO assigns lower prices to specific time slots, effectively aligning demand with grid stability objectives. The subsidy program supports the deployment of smallscale DERs. The ISO provides financial incentives for DER adoption, and users subsequently assess the economic feasibility of installing a set of DERs. If a user decides to install DERs, the user—now operating as a microgrid—can generate its own electricity, reducing reliance on the main grid and participating in energy trading with the ISO.

The ISO's multi-objective framework encompasses both operational and economic goals. From an operational perspective, the primary objective is to ensure grid stability by maintaining a balanced supply and demand. Specifically, in this problem, grid stability is assessed by observing fluctuations in peak load, where a lower recorded peak load is considered indicative of higher system stability. By managing DRPs, the ISO aims to mitigate extreme peak loads, thereby enhancing overall grid reliability. Economically, the ISO aims to minimize system-wide costs, including generation, transmission, and distribution expenses, while also promoting the integration of renewable energy sources. The ISO accounts for system-wide costs by structuring DRPs, which allocate budgets for managing electricity consumption patterns across the power grid system. These programs play a crucial role in optimizing cost efficiency while ensuring a reliable power supply. Moreover, as a non-profit entity, the ISO's primary focus tends to align more closely with operational objectives rather than with direct cost minimization. While economic considerations remain important, the ISO emphasizes grid stability and reliability, as these factors are fundamental to its role in maintaining an efficient and resilient electricity market.

To simplify the problem and to ensure practical applicability, this study operates under the following assumptions. The ISO is responsible for minimizing peak loads and for improving grid efficiency while managing DRPs such as subsidies and RTP mechanisms. Microgrids independently optimize their energy strategies but are influenced by the ISO's DRPs.

2.2. Distributed energy resources

In this problem, DERs are key components in decentralized power grid systems, focusing on their integration within microgrids under uncertain renewable energy conditions. The generation output of renewable energy sources (RESs), such as photovoltaic panels (PV) and wind turbines (WT), is inherently uncertain due to solar irradiation and wind speed fluctuations. To address uncertainty on RES, this study relies on pre-estimated data from prior research and forecasting methods to compute generation profiles, ensuring a realistic assessment of available renewable energy potential without explicitly modeling uncertainty

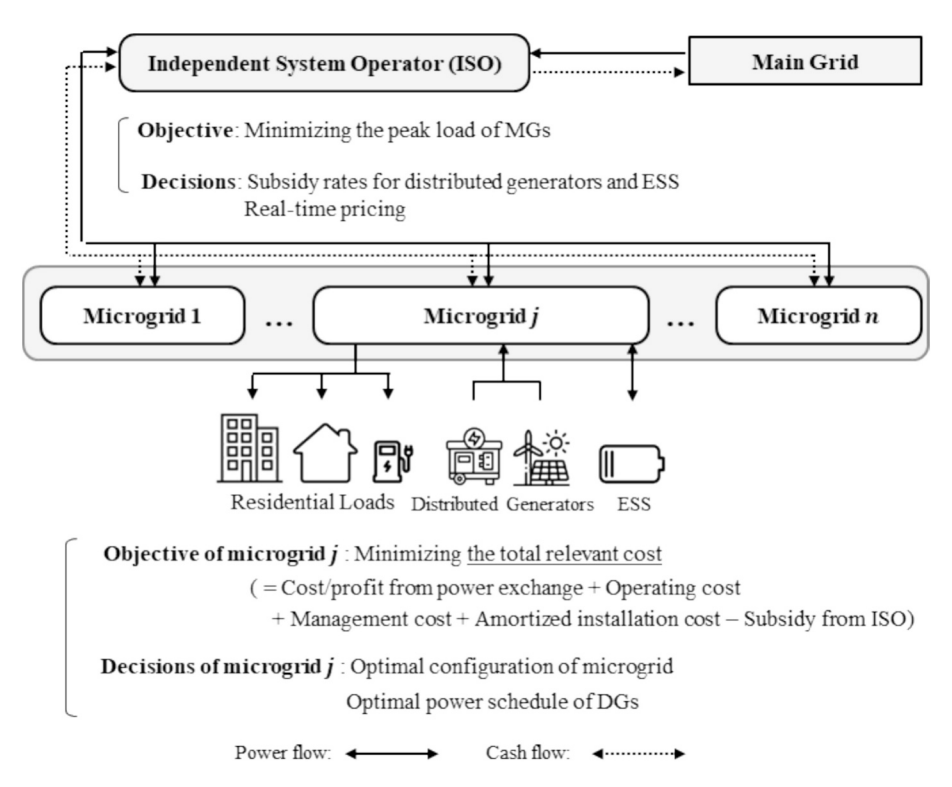


Fig. 1. Hierarchical structure of ISO and multiple microgrids.

[27-30].

The production capacity of renewable energy resources is intrinsically linked to the availability of essential natural resources, including but not limited to wind speed and solar irradiation [27]. This study leverages historical data to forecast the expected values of these parameters. Specifically, the anticipated power output from wind turbines is estimated based on wind speed forecasts, which follow a standard output curve defined as follows [28]:

$$P_t^{WT} = \begin{cases} 0, & 0 \leq v^t \leq v_{ci} \\ P_r \left(\frac{v^t - v_{ci}}{v_r - v_{ci}} \right), & v_{ci} \leq v^t \leq v_r \\ P_r, & v_r \leq v^t \leq v_{co} \\ 0, & v_{co} \leq v^t \leq v_{ci} \end{cases}$$

$$(1)$$

where v_{ci} , v_r , and v_{co} denote the cut-in, rated, and cut-out speeds of the wind turbine, respectively. P_r represents the rated power of the WT, and v^t is forecasted wind speed at time t. Similarly, the power output of each photovoltaic module is estimated based on the expected solar radiation using the following quadratic function [30]:

$$P_t^{PV} = A_{PV} s_t^2 + B_{PV} s_t + C_{PV} (2)$$

where s_t is the forecasted solar radiation at time t, and A_{PV} , B_{PV} , and C_{PV} are empirical coefficients derived from historical data. While these models are used to generate input data for optimization, it is acknowledged that the actual output of renewable DERs is subject to inherent uncertainty. To simplify the optimization problem and ensure computational tractability, deterministic forecasts for renewable outputs are adopted in this study, without explicitly modeling stochasticity. This assumption may limit the robustness of the results under real-world conditions, and the integration of stochastic or robust optimization is identified as a valuable direction for future research.

In addition to RESs, fuel cells (FCs), microturbines (MTs), and energy storage systems (ESSs) are considered in this study. Although these resources are not directly dependent on RESs, they are crucial in

maintaining grid stability by providing dispatchable power sources that enhance system flexibility in response to variable demand and intermittent renewable generation. Therefore, their installation and operation are incorporated into the problem formulation as part of the overall grid stability strategy.

Due to the small-scale nature of DERs, their deployment is treated as an operational decision rather than as a strategic investment. The introduced problem reflects DER systems' flexible and modular characteristics, where decisions regarding their operation and utilization are made on a shorter time scale compared to decisions made in large-scale power plants. The capital cost of DER installations is converted into daily equivalent costs using the *capital recovery factor* (CRF), ensuring consistency with the daily operational time horizon considered in this study.

2.3. Demand response programs and an ISO'S economic measures

The ISO implements two types of DRPs: RTP and the subsidy mechanism. The first DRP, RTP, allows the ISO to dynamically set retail electricity prices within predefined upper and lower bounds for each time slot. As an intermediary between the main grid and electricity users, the ISO procures electricity from the main grid and redistributes it based on user demand. The main grid's electricity procurement cost follows a predetermined system marginal price (SMP), while the RTP set by the ISO determines the retail price for users. The price difference or surplus resulting from the RTP mechanism is accounted for in the ISO's daily operational cost. The second DRP, the subsidy mechanism, provides financial support to electricity users by covering a portion of DER installation costs. The ISO first determines the subsidy rate for each DER, after which users assess the economic feasibility of DER adoption. As previously discussed in Section 2.2, installation costs are incorporated into the operational model using CRFs to ensure consistency with the daily operational time horizon. If a user installs DERs and generates surplus electricity, the ISO may purchase the excess energy at a price aligned with the SMP. This mechanism allows microgrids to actively participate in the energy market while ensuring a balance between supply and demand.

Specifically, the ISO's total daily operational cost is formulated as the sum of three primary components: (i) the price difference or surplus resulting from RTP-based electricity pricing, (ii) the cost of purchasing surplus electricity from DER-equipped users, and (iii) the total subsidy allocation for DER installations. By structuring these demand response programs, the ISO optimizes grid operations while maintaining cost efficiency and grid stability.

3. Multi-follower bilevel program model

In this section, the problem is formulated as a bilevel optimization model, capturing the hierarchical relationship between the ISO and microgrids. At the upper level, the ISO determines RTP and subsidy allocation strategies to minimize peak loads and operational costs. At the lower level, multiple electricity users or microgrids optimize their energy consumption, DER operations, and energy trading strategies to minimize their individual costs, guided by the ISO's signals. The hierarchical optimization structure effectively models the intricate tradeoffs and interactions between the ISO and microgrids.

3.1. Notations

Before presenting mathematical formulations, the notations used in the bilevel optimization model including indices, parameters, and variables, are introduced as follows. Indices represent key entities such as electricity users, time slots, and DER units. Parameters specify fixed values related to system constraints, costs, and efficiencies, while variables denote decision-making elements at both the ISO and microgrid levels.

Index and Set.

i	index for electricity user
t	index for time slot
k	index for DER unit
I	set of users
K	set of DER units, $K = \{MT, FC, WT, PV, ESS\}$
K_{DG}	set of DGs, $K_{DG} = \{MT, FC, WT, PV\}$
K_{RES}	set of DGs related with RES, $K_{RES} = \{WT, PV\}$

Parameters.

-		
	$lpha_k^{ m crf}$	capital recovery factors of DER unit k
	α_k^{gen}	energy conversion efficiency of DG $k \in K_{DG} \setminus K_{RES}$
	$lpha^{ m cha}$	charging efficiency of ESS
	$lpha^{ m dis}$	discharging efficiency of ESS
	$c_t^{ m price}$	electricity price at time t
	$\overline{c}_t^{ ext{rtp}}$	upper limit of real-tine pricing at time t
	$\underline{c}_t^{\text{rtp}}$	lower limit of real-tine pricing at time t
	$c_k^{ m oper}$	operating cost of DER unit k
	c_k^{main}	maintenance cost of DER unit k
	p_{it}	demand of electricity load of follower i at time t
	π_k	capital cost of DER unit k
	В	initial budget
	\overline{P}_k	maximum allowable power output of DER unit k
	\underline{P}_k	minimum allowable power output of DER unit k
	$\Delta \overline{P}_k$	ramp-up rate of DER unit k
	$\Delta \underline{P}_k$	ramp-down rate of DER unit k
	$P_{ikt}^{ m RES}$	estimated energy potential of RES k for follower i at time t
	$\overline{P}^{\mathrm{cha}}$	maximum charging rate of ESS
	$\overline{\textit{P}}^{ ext{dis}}$	minimum charging rate of ESS
	\overline{E}	maximum state of charge of ESS
	<u>E</u>	minimum state of charge of ESS

Variables.

p_{it}^{in}	the amount of electricity purchased by user i from the ISO at time t
$p_{it}^{ m out}$	the amount of electricity sold by user i to the ISO at time t
$p_{ikt}^{ m gen}$	the amount of electricity generated by DG k of user i at time t
	(continued on next column)

(continued)

$p_{it}^{ m cha}$	the amount of electricity charging into ESS of user i at time t
$p_{it}^{ m dis}$	the amount of electricity discharging from ESS of user i at time t
x_k^{sub}	subsidy rate associated with DER unit k
x_t^{rtp}	electricity price determined by the ISO at time t
y_{ik}	binary variable: 1 if user i installs DER k , otherwise 0

3.2. Leader's optimization problem

The leader's optimization problem focuses on the ISO's multiobjective optimization goals of enhancing power grid operational efficiency and cost optimization. These objectives are addressed using the ε -constraint method, guiding the ISO in determining RTP and subsidy levels to influence user behavior while balancing budget constraints and grid stability requirements.

The ISO's first objective in the bilevel optimization problem is to minimize the peak load throughout the planning period, which in this study is defined as one day. The leader's objective function for the grid stability requirements is formulated in Eq. (3), where the term $\sum_{\forall i} (p_{it}^{\text{in}} - p_{it}^{\text{out}})$ represents the total power transaction volume for all electricity users at time t.

$$\min \max_{\forall t \in T} \left\{ \sum_{\forall i} \left(p_{it}^{\text{in}} - p_{it}^{\text{out}} \right) \right\}$$
 (3)

The second objective of the ISO, represented in Eq. (4), is to minimize the total daily operational cost while ensuring that it does not exceed the initial budget B. This formulation is also based on the ε -constraint method. The daily operational cost consists of the profit (or loss) from power transactions and the total subsidies paid to users for DER installations. Eq. (5) describes the profit from power redistribution and trading. The first term represents revenue (or loss) from the difference between the wholesale price (SMP) and the retail price (RTP) set by the ISO. The second term accounts for the cost of purchasing surplus power from the users. Eq. (6) calculates the total subsidies provided to users who install DERs.

$$s.t. \sum_{\forall i} \left[\sum_{\forall t} C_{it}^{\text{prof}} + \sum_{\forall k} C_{ik}^{\text{sub}} \right] \leq B$$
 (4)

$$C_{it}^{\text{prof}} = (c_t^{\text{price}} - x_t^{\text{rtp}}) p_{it}^{\text{in}} + c_t^{\text{price}} p_{it}^{\text{out}}, \quad \forall i, \forall t$$
 (5)

$$C_{ik}^{\text{sub}} = \alpha_k^{\text{crf}} \pi_k \mathbf{x}_k^{\text{sub}} \mathbf{y}_{ik}, \ \forall k \in K$$
 (6)

The decision variables on RTP and subsidy rates are defined in Eqs. (7)–(8).

$$\underline{c}_{t}^{\text{rtp}} \le \mathbf{x}_{t}^{\text{rtp}} \le \overline{c}_{t}^{\text{rtp}} \forall t \tag{7}$$

$$0 < \chi_k^{\text{sub}} < 1 \forall k \in K \tag{8}$$

3.3. Followers' optimization problems

The followers' problems represent the decision-making processes of individual microgrids or electricity users. Each user optimizes their energy usage, DER operations, and participation in energy trading based on the pricing and subsidy signals provided by the ISO. The follower's objective is to minimize individual operational costs while adhering to local constraints such as energy balance and DER capacity.

The objective function in Eq. (9) represents the cost function of the followers. The associated variables include the cost function for power transactions with the ISO, the operational cost functions for MT and FC, the maintenance cost functions for PV and WT, the maintenance cost function for energy storage systems, and the investment cost function for DER units. These functions are presented in Eqs. (10)–(14).

$$\min \sum_{\forall t} \left(C_{it}^{\text{exch}} + \sum_{\forall k \in K} C_{ikt}^{\text{DER}} \right) + C_{ik}^{\text{inv}}$$
(9)

$$s.t.C_{it}^{\text{exch}} = x_t^{\text{rtp}} p_{it}^{\text{in}} - c_t^{\text{price}} p_{it}^{\text{out}}, \quad \forall t$$
 (10)

$$C_{ikr}^{\text{DER}} = \left(c_{k}^{\text{oper}} / \alpha_{k}^{\text{gen}}\right) p_{ikr}^{\text{gen}}, \forall k \in K \backslash K_{RES}, \forall t$$
(11)

$$C_{ikr}^{\text{DER}} = c_k^{\text{main}} p_{ikr}^{\text{gen}}, \forall k \in K_{RES}, \forall t$$
(12)

$$C_{ikt}^{\text{DER}} = c_{\text{ESS}}^{\text{main}} \left(p_{it}^{\text{cha}} + p_{it}^{\text{dis}} \right), k = \text{ESS}, \forall t$$
(13)

$$C_{ik}^{\text{inv}} = \alpha_k^{CRF} \pi_k (1 - x_k^{\text{sub}}) y_{ik}, \forall k \in K$$
(14)

The power generation capabilities of dispatchable resources, such as MT and FC, are contingent upon their installation within the microgrid. These resources operate within defined capacity limits, with their output constrained by the maximum \overline{P}_k and minimum \underline{P}_k allowable power levels. In contrast, non-dispatchable resources, including PV and WT, generate active power based on their estimated energy potential, P_{ikt}^{RES} , which is forecasted from environmental conditions like solar irradiance and wind speed. However, the availability of these renewable resources does not guarantee consistent output, even when connected to the microgrid. Furthermore, the rate at which power output can change is regulated by ramp rate constraints, ensuring a smooth transition in power generation. These constraints include the ramp-up $\Delta \overline{P}_k$ and ramp-down $\Delta \underline{P}_k$ limits, which help maintain grid stability during dynamic operational changes. The detailed constraints related to DGs are presented in Eqs. (15)–(18).

$$P_k y_{ik} \le p_{ikt}^{\text{gen}} \le \overline{P}_k y_{ik}, \forall k \in K_{\text{DG}} \setminus K_{RES}, \forall t$$
(15)

$$p_{ikr}^{\text{gen}} \le P_{ikr}^{\text{RES}} y_{ik}, \forall k \in K_{\text{RES}}, \forall t$$
 (16)

$$p_{i,k,1}^{\text{gen}} \le \Delta \overline{P}_k y_{ik}, \forall k \in K_{\text{DG}}$$

$$\tag{17}$$

$$\Delta \underline{P}_k y_{ik} \le p_{ikt}^{\text{gen}} - p_{ikt-1}^{\text{gen}} \le \Delta \overline{P}_k y_{ik}, \forall k \in K_{\text{DG}}, \forall t = 2...24$$
 (18)

The charging and discharging rates of ESS are restricted by their respective maximum allowable rates, ensuring that the system operates within safe and efficient limits. Furthermore, the energy level within the ESS at any given time t must remain between its minimum capacity \underline{E} and maximum capacity \overline{E} . These constraints ensure that the ESS operates within its designed parameters. Additionally, since an ESS stores direct current power, the system accounts for charging and discharging efficiencies $\alpha^{\rm cha}$ and $\alpha^{\rm dis}$, converting alternating current power into storable energy. At time t, the power that can be charged or discharged is further constrained by the upper bounds, $\overline{P}^{\rm cha}$ and $\overline{P}^{\rm dis}$, respectively. The ESS constraints are formulated in detail in Eqs. (19)–(21), which incorporate these operational boundaries.

$$0 \le p_{it}^{\text{cha}} \le \overline{P}^{\text{cha}} y_{i,\text{ESS}}, \forall t$$
 (19)

$$0 \le p_{it}^{\text{dis}} \le \overline{P}^{\text{dis}} \gamma_{i,\text{ESS}}, \forall t \tag{20}$$

$$\underline{E}\mathbf{y}_{\mathrm{ESS}} \leq \sum_{a=1}^{t} \left(\alpha^{\mathrm{cha}} p_{ia}^{\mathrm{cha}} - p_{ia}^{\mathrm{dis}} / \alpha^{\mathrm{dis}} \right) \leq \overline{E}\mathbf{y}_{\mathrm{ESS}}, \forall t \tag{21}$$

Eq. (22) represents the constraint on energy balance. The total power transacted with the ISO and the power generated by distributed generators must equal the energy demand and the charging or discharging volume of follower i at time t. A critical aspect of the constraint is that at any given time t, power transactions with the ISO must occur through only one channel—purchasing or selling electricity, but not both simultaneously. The same condition applies to charging and discharging operations for ESS. While the restriction is automatically enforced by the objective function's coefficient settings during the follower's

optimization process, it is important to note that ignoring the follower's objective function could lead to a situation where both channels simultaneously hold non-negative values.

$$p_{it}^{\text{in}} - p_{it}^{\text{out}} + \sum_{i,t} p_{ikt}^{\text{gen}} = p_{it} + \alpha^{\text{cha}} p_{it}^{\text{cha}} - \alpha^{\text{dis}} p_{it}^{\text{dis}}, \forall t$$
 (22)

All continuous decision variables of the followers, such as p_{ir}^{in} , p_{ir}^{out} , p_{ik}^{gen} , p_{ik}^{cha} , and p_{ik}^{dis} are constrained to be non-negative. However, certain solutions obtained from the follower's optimization problem may be infeasible for the leader's problem, even if the decision variables satisfy the constraints. This discrepancy arises when the follower's decision variables conflict with constraints specific to the leader's optimization problem. In the proposed bilevel model, conflict arises when the follower's response to DRPs exceeds the ISO's constrained budget. Such a conflict prevents the use of backward induction—a sequential solution method for leader-follower models that involves determining the follower's best response to the leader's decision. Backward induction relies on the assumption that the follower's solution space is entirely compatible with the leader's constraints, which is not guaranteed in the addressed problem. To address this challenge and to ensure a feasible solution, the study adopts a bilevel programming approach. Specifically, the bilevel program is transformed into an equivalent single-level optimization problem, as suggested by Kovács and Kovács [31]. However, the reformulation technique cannot be directly applied to the presented bilevel program due to the inclusion of discrete decision variables in the follower's problem, which violates the assumptions of standard reformulation techniques based on KKT conditions [32–34]. To overcome the limitations, the next section introduces a reformulation-anddecomposition algorithm. The solution approach separates the bilevel program into a master problem and subproblems, ensuring compatibility between the leader's and follower's constraints while maintaining computational tractability.

4. Reformulation-and-decomposition algorithm

This section introduces a solution approach to solving the bilevel problem for multiple electricity users interacting with an ISO. The algorithm leverages reformulation and decomposition techniques to address the complexity introduced by multiple followers with diverse decision variables and objectives. The proposed method ensures computational efficiency and scalability by transforming the bilevel problem into a single-level optimization problem and then breaking it into smaller, tractable subproblems. The process accounts for both continuous and discrete variables while maintaining the hierarchical structure of leader-follower interactions, ensuring accurate and practical solutions for grid operations.

4.1. Reformulation

To address the hierarchical nature of the bilevel optimization problem, the original model is reformulated into a single-level problem. This reformulation replaces the follower's problem with its KKT conditions, allowing the ISO to incorporate the followers' optimal responses in its decision-making. However, KKT conditions are applicable only if the follower's problem is convex and satisfies strong duality [35,36]. In this study, the presence of discrete decision variables in the follower's problem poses a challenge to directly applying KKT-based reformulation.

To resolve this issue, each follower's problem is decomposed into manageable subproblems. Specifically, the discrete variables of the followers y_{ik} are treated as constant during the reformulation procedure. By fixing these variables, the follower's problem is decomposed into several subproblems, and each subproblem becomes a linear program, enabling the use of KKT conditions to approximate the follower's optimal responses. The bilinear terms $x_t^{\text{rtp}}p_{it}^{\text{in}}$ and $x_k^{\text{sub}}y_k$ in the follower's

objective function are treated as linear term or constant because the ISO's decision variables are fixed as constants from the follower's perspective. The reformulation of decomposed subproblems ensures that the problems remain both mathematically rigorous and computationally tractable

The reformulation is performed by substituting a decomposed subproblem for each follower i as defined in Eqs. (9)–(21) with its corresponding KKT conditions. As a result of substitution, the stationarity conditions for each follower i are expressed in Eqs. (23)–(32).

$$x_t^{\text{rtp}} + v_{i,t}^{\text{C20}} - u_{i,t}^{\text{in}} = 0, \forall t$$
 (23)

$$-c_t^{\text{price}} - v_{i,t}^{\text{C20}} - u_{i,t}^{\text{out}} = 0, \forall t$$
 (24)

$$\begin{split} c_i^{\text{oper}} \middle/ \alpha_i^{\text{gen}} + c_i^{\text{main}} + u_{i,k,t}^{\text{C20}} + u_{i,k}^{\text{C20}} + u_{i,k,t+1}^{\text{C20l}} - u_{i,k,t+1}^{\text{C16u}} + \nu_{i,t}^{\text{C20}} - u_{i,k,t}^{\text{gen}} = 0, \forall k \\ \in K_{\text{RES}}, t = 1 \end{split}$$

(25)

$$\begin{split} c_{i}^{\text{oper}} \middle/ \alpha_{i}^{\text{gen}} + c_{i}^{\text{main}} + u_{i,k,t}^{\text{C14}} + u_{i,k,t+1}^{\text{C16l}} - u_{i,k,t}^{\text{C16l}} + u_{i,k,t}^{\text{C16l}} - u_{i,k,t+1}^{\text{C16u}} + v_{i,t}^{\text{C20}} - u_{i,k,t}^{\text{gen}} \\ &= 0, \forall k \in K_{\text{RES}}, \forall t = 2, ..., 23 \end{split}$$

$$c_{i}^{\text{oper}} / \alpha_{i}^{\text{gen}} + c_{i}^{\text{main}} + u_{i,k,t}^{\text{C14}} - u_{i,t}^{\text{C16l}} + u_{i,t}^{\text{C16l}} + v_{i,t}^{\text{C20}} - u_{i,k,t}^{\text{gen}} = 0, \forall k \in K_{\text{RES}}, t = 24$$
(27)

$$\begin{split} c_i^{\text{oper}} \middle/ \alpha_i^{\text{gen}} + c_i^{\text{main}} - u_{i,k,t}^{\text{C13}l} + u_{i,k,t}^{\text{C13}u} + u_{i,k,t+1}^{\text{C16}l} - u_{i,k,t+1}^{\text{C16}l} + \nu_{i,t}^{\text{C20}} - u_{i,k,t}^{\text{gen}} = 0, \forall k \\ \in K \backslash K_{\text{RES}}, t = 1 \end{split}$$

(28)

$$\begin{split} c_i^{\text{oper}} \middle/ \alpha_i^{\text{gen}} + c_i^{\text{main}} - u_{i,k,t}^{\text{C13}l} + u_{i,k,t}^{\text{C13}u} + \left(u_{i,k,t+1}^{\text{C16}l} - u_{i,k,t}^{\text{C16}l} + u_{i,k,t}^{\text{C16}u} - u_{i,k,t+1}^{\text{C16}u} \right) + \nu_{i,t}^{\text{C20}} - u_{i,k,t}^{\text{gen}} \\ = 0, \forall k \in K \setminus K_{\text{RES}}, \forall t = 2, \dots, 23 \end{split}$$

(29)

$$c_{i}^{\text{oper}} / a_{i}^{\text{gen}} + c_{i}^{\text{main}} - u_{i,k,t}^{\text{C13}l} + u_{i,k,t}^{\text{C13}u} - u_{i,t}^{\text{C16}l} + u_{i,t}^{\text{C16}u} + v_{i,t}^{\text{C20}} - u_{i,k,t}^{\text{gen}} = 0, \forall k$$

$$\in K \setminus K_{\text{RES}}, t = 24$$
(30)

$$c_{\rm ESS}^{\rm main} + u_{i,t}^{\rm C17} - \sum\nolimits_{a=t}^{nT} \left(\alpha^{\rm cha} u_{i,a}^{\rm C19u} - \alpha^{\rm cha} u_{i,a}^{\rm C19l}\right) - v_{i,t}^{\rm C20} - u_{i,t}^{\rm cha} = 0, \forall t \tag{31}$$

$$c_{\rm ESS}^{\rm main} + u_{i,t}^{\rm C17} + \sum\nolimits_{a=t}^{nT} \left(u_{i,a}^{\rm C18i} \middle/ \alpha^{\rm dis} - u_{i,a}^{\rm C18u} \middle/ \alpha^{\rm cha}\right) + v_{i,t}^{\rm C19} - u_{i,t,s}^{\rm dis} = 0, \forall t \qquad (32)$$

where the notation u represents the non-negative dual variables associated with inequality constraints in Eqs. (15)–(21) and the non-negative primal variables, while the notation v describes the unrestricted dual variable corresponding to the equality constraint in Eq. (22).

Next, the complementary slackness conditions are formulated as shown in Eqs. (33)–(42). These conditions ensure that the primal and dual solutions satisfy the equilibrium necessary for bilevel optimization, providing a coherent framework for integrating follower decisions into the leader's problem. In contrast to traditional methods that rely on Big-M formulation to linearize bilinear terms, this study employs SOS1 constraints to manage the discrete nature of the decision variables. SOS1 constraints are particularly advantageous as they explicitly enforce sparsity, ensuring that only one variable in a predefined set can take a nonzero value at any given time. This property simplifies the reformulation process and eliminates the need for arbitrary scaling factors inherent in Big-M formulation. The remaining conditions, such as primal feasibility, are associated with Eqs. (15)–(22). The dual feasibility conditions are associated with the dual variables introduced in Eqs. (23)–(32).

$$0 \le u_{i,t}^{C13l} \perp \left(\underline{P}_k y_{i,k} - p_{i,k,t}^{\text{gen}} \right) \le 0, \forall k \in K_{\text{DG}} \setminus K_{\text{RES}}, \forall t$$
(33)

$$0 \le u_{i,t}^{C13u} \perp \left(p_{i,k,t}^{\text{gen}} - \overline{P}_k y_{i,k} \right) \le 0, \forall k \in K_{\text{DG}} \setminus K_{\text{RES}}, \forall t$$
(34)

$$0 \le u_{i,t}^{C14} \perp \left(p_{i,k,t}^{\text{gen}} - P_{i,k,t}^{\text{RES}} \mathbf{y}_{i,k} \right) \le 0, \forall k \in K_{\text{RES}}, \forall t$$
(35)

$$0 \le u_{i,t}^{C15} \perp \left(p_{i,k,1}^{\text{gen}} - \Delta \overline{P}_i y_i \right) \le 0, \forall k \in K_{\text{RES}}, t = 1$$
(36)

$$0 \le u_{i,t}^{C16l} \perp \left(\Delta \underline{P}_k y_{i,k} - p_{i,k,t}^{\text{gen}} + p_{i,k,t-1}^{\text{gen}} \right) \le 0, \forall k \in K_{\text{DG}}, \forall t = 2, ..., 24$$
 (37)

$$0 \leq u_{i,t}^{\text{C16}u} \perp \left(p_{i,k,t}^{\text{gen}} - p_{i,k,t-1}^{\text{gen}} - \nabla \overline{P}_k \mathbf{y}_{i,k} \right) \leq 0, \forall k \in K_{\text{DG}}, \forall t = 2, ..., 24$$
 (38)

$$0 \le u_{i,t}^{C17} \perp \left(p_{i,t}^{\text{cha}} - \overline{P}^{\text{cha}} y_{i,\text{ESS}} \right) \le 0, \forall t$$
(39)

$$0 \le u_{i,t}^{C18} \perp \left(p_{i,t}^{\text{dis}} - \overline{P}^{\text{dis}} y_{i,\text{ESS}} \right) \le 0, \forall t$$

$$\tag{40}$$

$$0 \le u_{i,a}^{\text{C19l}} \bot \underline{E} y_{\text{ESS}} - \sum_{\alpha=1}^{t} \left(\alpha^{\text{cha}} p_{i,a}^{\text{cha}} - p_{i,a}^{\text{dis}} \middle/ \alpha^{\text{dis}} \right) \le 0, \forall t$$
 (41)

$$0 \le u_{i,a}^{C19u} \perp \sum_{a=1}^{t} \left(\alpha^{\text{cha}} p_{i,a}^{\text{cha}} - p_{i,a}^{\text{dis}} \middle/ \alpha^{\text{dis}} \right) - \overline{E} \mathbf{y}_{\text{ESS}} \le 0, \forall t$$
 (42)

In the following subsections, the decomposition technique used to apply the KKT conditions to each subproblem within the proposed solution approach is described. It is important to distinguish between two levels of decomposition: one applied to the follower's problem in the reformulation process and the other to the overall bilevel model. Specifically, the decomposition of the follower's problem involves fixing discrete variables to enable the application of strong duality, thereby reformulating the lower-level problem. On the other hand, the decomposition technique applied to the bilevel model is designed to control the growth of variables and constraints as the problem size increases, ensuring computational efficiency during the algorithmic search process.

4.2. Generalized benders decomposition

In the previous subsection, the KKT conditions were introduced to replace each decomposed subproblem by fixing discrete variables. However, as the number of subproblems increases, as the number of subproblems increases with the growth in discrete variable combinations, the number of variables and constraints in the bilevel model incorporating these KKT conditions increases exponentially. To address this issue efficiently, a generalized Benders decomposition technique is applied. For clarity, vector-based notations for the decision variables are defined below before presenting the decomposition procedure.

$$\boldsymbol{x} = \left[\boldsymbol{x}_{k}^{\text{sub}}, \boldsymbol{x}_{t}^{\text{rtp}}\right]^{T}, \boldsymbol{p} = \left[\boldsymbol{p}_{it}^{\text{in}}, \boldsymbol{p}_{it}^{\text{out}}, \boldsymbol{p}_{ikt}^{\text{gen}}, \boldsymbol{p}_{it}^{\text{cha}}, \boldsymbol{p}_{it}^{\text{dis}}\right]^{T}, \text{ and } \boldsymbol{y} = \left[\boldsymbol{y}_{ik}\right]^{T}$$
(43)

The decomposition process divides the original bilevel model into a master problem and subproblems. The master problem, denoted as **MP**, incorporates the KKT conditions and optimality cuts for all subproblems of each follower, as formulated in (44)–(51). In the master problem, p_0 and y_0 are auxiliary decision variables for checking the feasibility of followers' responses and the optimality from KKT conditions. The auxiliary decision variables p_s are used to determine the followers' best response to the leader's decision x. Each subproblem is enumerated with the combination of the constant discrete variables y_s and for follower i. The KKT conditions in (51) impose constraints on the follower's best response for each subproblem defined by y_s . Specifically, these conditions ensure that the feasible solution p_s and y_s , are used in the master problem to restrict the auxiliary decision variables p_0 and y_0 through

optimality cuts associated with the follower's objective function in (51).

min.
$$F(\mathbf{x}, \mathbf{p}_0, \mathbf{y}_0) : \text{Eq.}(3)$$
 (44)

s.t.
$$G(x, p_0, y_0) \le 0$$
: Eqs.(4) and (7)–(8) (45)

$$H(x, p_0, y_0) = 0 : \text{Eqs.}(5)-(6)$$
 (46)

$$g_i(x, p_0, y_0) \le 0, \forall i : \text{Eqs.}(15)-(21)$$
 (47)

$$h_i(x, p_0, y_0) = 0, \forall i : \text{Eqs.}(10) - (14) \text{ and } (22)$$
 (48)

$$\boldsymbol{p}_0 \ge \boldsymbol{0} \tag{49}$$

$$\mathbf{y}_0 \in \mathbb{B}$$
 (50)

$$\begin{cases} f_i(\mathbf{x}, \mathbf{p}_0, \mathbf{y}_0) \leq f_i(\mathbf{x}, \mathbf{p}_s, \mathbf{y}_s) \\ \nabla_{\mathbf{p}_s} f_i(\mathbf{x}, \mathbf{p}_s, \mathbf{y}_s) + \nabla_{\mathbf{p}_s} \mathbf{g}_i(\mathbf{x}, \mathbf{p}_s, \mathbf{y}_s)^T \mathbf{u} + \nabla_{\mathbf{p}_s} \mathbf{h}_i(\mathbf{x}, \mathbf{p}_s, \mathbf{y}_s)^T \mathbf{v} = \mathbf{0} \\ \mathbf{g}_i(\mathbf{x}, \mathbf{p}_s, \mathbf{y}_s) \leq \mathbf{0} \\ \mathbf{h}_i(\mathbf{x}, \mathbf{p}_s, \mathbf{y}_s) = \mathbf{0} \\ \mathbf{g}_i(\mathbf{x}, \mathbf{p}_s, \mathbf{y}_s)^T \mathbf{u} = \mathbf{0} \\ \mathbf{u} \geq \mathbf{0} \\ \mathbf{p}_s \geq \mathbf{0} \end{cases}$$

where $F(\bullet)$, $G(\bullet)$, and $H(\bullet)$ denote the objective function, inequality constraints, and equality constraints of the ISO, respectively. The notations $f_i(\bullet)$, $g_i(\bullet)$, and $h_i(\bullet)$ signify the objective function, inequality constraints, and equality constraints of follower i, (respectively)

However, the set S of discrete variable combinations can grow significantly depending on the problem instance, leading to an increase in the model size. To address this, a **Benders decomposition-based approach is adopted, which** iteratively explores solutions by starting from a **relaxed master problem** (**RMP**), defined over a limited set S_0 , and progressively adds new discrete variable combinations for the followers. These combinations are explored through a **two-stage sub-problem framework**.

The first subproblem, denoted as SP1, determines the follower's best response corresponding to the leader's decision \boldsymbol{x}^* given from RMP. Specifically, SP1 is equivalent to the follower's optimization problem defined by the objective function in Eq. (9) and the associated constraints in Eqs. (10)–(22). Let $(\boldsymbol{p}_0^*, \boldsymbol{y}_0^*)$ be the best solution for SP1. The corresponding objective function value $f_i(\boldsymbol{x}^*, \boldsymbol{p}_0^*, \boldsymbol{y}_0^*)$ is set as θ_i^* . The second subproblem, denoted SP2, explores a feasible solution from the leader's perspective while keeping \boldsymbol{x}^* fixed and ensuring that the follower's best solution obtained from SP1 is satisfied. The SP2 formulation is given by Eqs. (44)–(50) along with Eq. (52). Eq. (52) integrates the best objective value θ_i^* obtained from SP1, ensuring that the leader's decision-making process properly accounts for the follower's optimal behavior.

$$f_i(\mathbf{x}, \mathbf{p}_0, \mathbf{y}_0) \le \theta_i^*, \forall i \tag{52}$$

In this Benders decomposition-based technique, the RMP always provides a relaxed solution, whereas SP2 searches for a feasible primal solution or reports infeasibility. The iterative process continues until no further discrete variable combinations y_s need to be added to the master problem. Specifically, if the solutions obtained from RMP and SP2 converge to the same result, the procedure terminates, yielding the best solution. Alternatively, the procedure may terminate with an alternative solution where the follower's optimal response does not satisfy the leader's constraints. The latter case is further discussed in detail in the computational experiments section. To systematically implement this decomposition-based technique, the detailed algorithmic procedure is outlined in the following section.

4.3. Algorithm procedures

The flowchart of the proposed reformulation-decomposition algorithm is illustrated in Fig. 2. The algorithm begins with an initialization phase where key variables such as the lower bound LB and upper bound UB are initialized to negative and positive infinity, respectively, and a tolerance level of ε is set to ensure convergence. An empty set S_0 (or S_k) is also initialized to store discrete variable combinations explored during the iterations. Next, the current lower bound is updated based on the relaxed solution of the RMP. Subsequently, the feasibility of the leader's best solution x^* from RMP is verified with respect to the bilevel optimization problem. This is done through solving two subproblems, SP1 and SP2, which ensure that the leader's decisions are compatible with the followers' optimal responses. Specifically, SP1 evaluates the objective function value corresponding to the followers' optimal response to the leader's decision x^* . Meanwhile, SP2 provides a solution to the

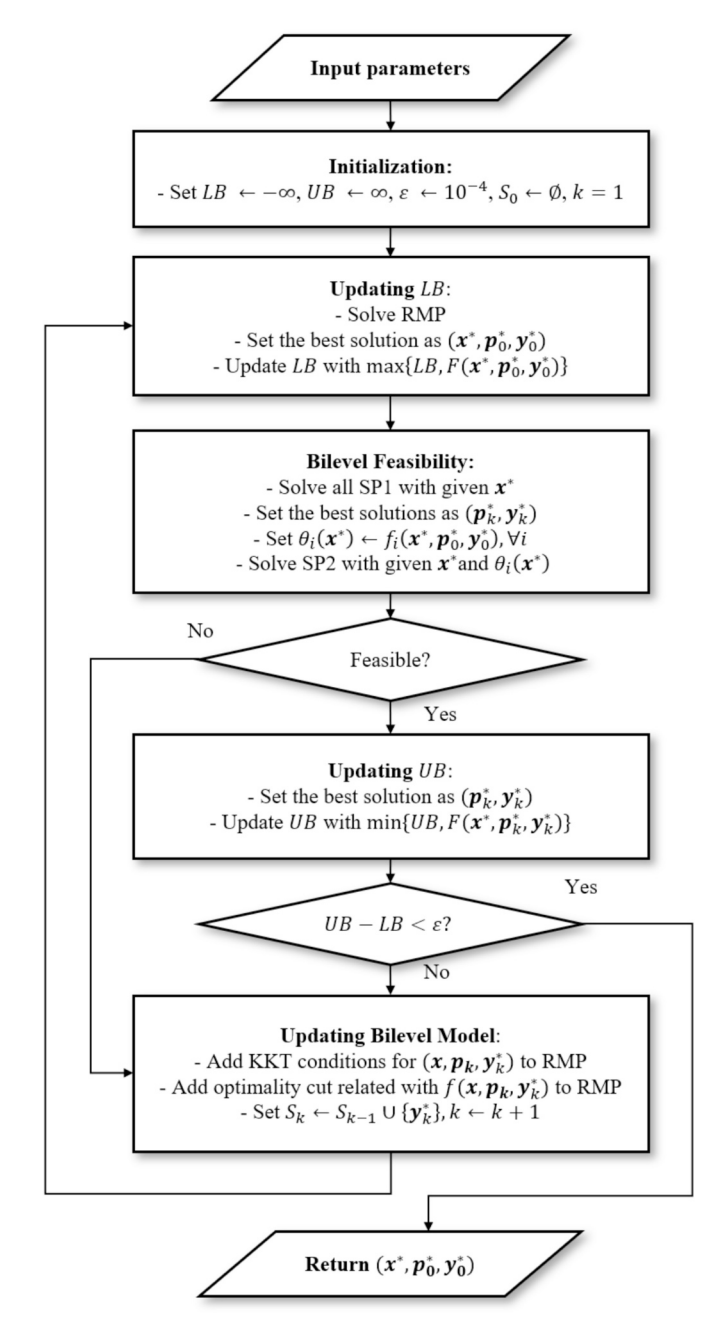


Fig. 2. Flowchart of the reformulation-and-decomposition algorithm.

original problem by incorporating the obtained follower's objective function value while keeping \mathbf{x}^* fixed, without imposing restrictions on the follower's decisions. If an alternative solution exists in **SP2**, it satisfies feasibility and is used to update the primal bound. Next, the gap between the dual bound and the primal bound is computed, and if the convergence criterion is met, the best solution from either **RMP** or **SP2** is returned. If the convergence condition is not satisfied, the combination of values of \mathbf{y}_0^* is added to the set S_0 (or S_k), and the corresponding KKT conditions and optimality cut, as defined in Eq. (51), are incorporated into **RMP**. However, if **SP2** results in infeasibility, the combination of values of \mathbf{y}_0 obtained from **SP1** is instead used to update the set S_0 (or S_k) and Eq. (51). This iterative procedure continues until either (i) the dual-primal gap falls below the predefined tolerance ϵ , or (ii) neither **SP1** nor **SP2** identifies a new \mathbf{y}_0^* .

The proposed algorithm offers several key advantages in addressing the challenges of solving bilevel optimization problems, particularly in multi-follower scenarios. By leveraging SOS1 constraints, the algorithm effectively incorporates discrete decision variables without the computational burden associated with Big-M relaxation. This approach enhances numerical stability and eliminates reliance on arbitrary scaling factors, streamlining the solution process for problems involving mixedinteger variables. Another key advantage of the algorithm is its scalability. By decomposing the problem into a master problem and manageable subproblems, the algorithm maintains computational efficiency even as the number of followers and the complexity of decision variables grow. This scalability is essential for real-world applications where the number of stakeholders and grid components can be substantial. The algorithm preserves the hierarchical structure of leaderfollower interactions by carefully structuring the reformulation process. By fixing discrete variables during the reformulation step, the algorithm ensures compatibility with convex optimization techniques while accurately modeling the interdependent decisions of the leader and followers. This approach maintains the integrity of the bilevel structure while enabling efficient computation.

5. Computational experiments

To demonstrate the applicability of the proposed reformulation-and-decomposition algorithm, computational case studies are conducted on the design of an upcoming microgrid as a pilot test. These experiments first examine the effects of different DRP settings in the bilevel optimization problem along with the computational performance of the algorithm. Next, the Pareto curve for the ISO's objectives is analyzed to assess the trade-off between the grid stability and the economic measures. Finally, managerial insights are provided regarding the implementation of the algorithm within the hierarchical structure of interactions between the ISO and microgrids. This analysis demonstrates the practical applicability of the proposed approach to real-world microgrid planning.

5.1. Problem instance and experimental setting

Electricity demand for each user is generated based on a normal distribution. The mean hourly electricity demand μ_t is set according to historical data from the literature, while the standard deviation σ_t is defined as a fraction of μ_t where the variability factor is empirically set to 0.15 to account for consumption variability. The resulting demand values for multiple users follow:

$$p_{it} \sim N(\mu_t, \sigma_t^2), \sigma_t = \beta \bullet \mu_t \tag{53}$$

where β is the variability factor ensuring diversity in electricity consumption.

Table 1 presents the mean hourly electricity demand derived from referenced datasets, along with the generated demand profiles for three electricity users. The potentials of PV and WT, which electricity users

Table 1
Time-series data of electricity prices, RES potentials, and electricity demand.

Time (hour)	$\mu_t(kW)$	User 1 (kW)	User 2 (kW)	User 3 (kW)	PV (kW)	WT (kW)	SMP (¢/kWh)
0	52	44.4	46.7	53.8	0	1.785	0.23
1	50	42.1	47.6	52.5	0	1.785	0.19
2	50	41.3	47.7	45.9	0	1.785	0.14
3	50	45.4	61.9	45.8	0	1.785	0.12
4	56	52.8	60.3	52.7	0	1.785	0.12
5	63	53.8	64.2	57.6	0	0.915	0.20
6	70	70.7	73.8	68.1	0	1.785	0.23
7	75	72.0	72.7	66.5	0.2	1.305	0.38
8	76	78.0	67.9	73.4	3.75	1.785	1.50
9	80	82.1	72.3	74.9	7.53	3.090	4.00
10	78	78.0	77.2	79.6	10.45	8.775	4.00
11	74	71.9	78.4	80.5	11.95	10.41	4.00
12	72	70.5	78.0	81.2	23.90	3.915	1.50
13	72	70.1	79.0	77.1	21.05	2.370	4.00
14	76	77.2	78.2	76.8	7.88	1.785	2.00
15	80	80.3	80.3	81.5	4.23	1.305	1.95
16	85	89.5	83.2	82.5	0.55	1.785	0.60
17	88	86.1	95.0	89.7	0	1.785	0.41
18	90	86.6	87.1	84.9	0	1.302	0.35
19	87	78.8	86.9	83.8	0	1.785	0.43
20	78	76.4	80.8	81.8	0	1.301	1.17
21	71	72.0	70.5	65.1	0	1.301	0.54
22	65	66.5	60.5	59.7	0	0.915	0.30
23	56	57.1	55.2	51.9	0	0.615	0.26

can assess for installation, are based on the data from the literature [37]. The potential of RES is assumed to be identical across all users when they install PV or WT units. The SMPs represent the electricity price accessed by the ISO. In this study, the price at which the ISO purchases surplus electricity from users is set equal to the SMPs. The lower/upper limit for the ISO's RTP is set according to the minimum/maximum SMP values in Table 1. Specifically, the lower limit is 0.5 times the minimum SMP, while the upper limit is 1.5 times the maximum SMP. The maximum budget allocated for supporting the DRPs is set to \$100. To analyze the impact of budget constraints on the proposed bilevel optimization problem, the ε -constraint method is applied. Accordingly, the budget B varies from 0 to 100 in increments of 5 to assess the trade-off between the grid stability and the economic measures.

Table 2 summarizes the capital, operational, and technical specifications of the DER units, with reference to established data sources [37-40]. The table includes capital costs, operating costs, and maintenance costs associated with each DER unit. The capital costs are converted into daily equivalent values using CRFs, derived from annual costs computed with a standard annuity formula using an interest rate of 6 % and economic lifetimes of 10 and 3 years for DG and ESS, respectively. These values are adopted from Sufyan et al. [39], and the resulting annual CRFs are divided by 365 to yield daily costs of 0.000372 and 0.001025. Operating costs reported in Table 2 inherently reflect both fuel prices and fuel-to-electricity conversion efficiency of the generation units (e.g., MT and FC), and therefore, explicit modeling of thermal efficiency is not required. Maintenance costs are adopted from Qi et al. [38] for most units, while the ESS maintenance cost is referenced from Sufyan et al. [39], which incorporates battery degradation modeling. Technical constraints include the minimum and

 Table 2

 Economic and technical parameters of the DER units.

DER unit	MT	FC	PV	WT	ESS
Capital cost (K\$/DER unit) [39,40]	27	60	75	32.25	33
Operating cost (¢/kWh) [39]	0.4	0.2	-	-	-
Maintenance cost (¢/kWh) [38,39]	0.12	0.04	0.11	0.08	0.02
Min power (kW) [37]	6	3	0	0	-30
Max power (kW) [37]	30	30	25	15	30
Ramp-up rate (kW) [39]	140	120	-	-	20
Ramp-down rate (kW) [39]	-30	-60	-	-	-60

maximum power output of each unit. PV and WT have zero minimum output, reflecting their dependency on solar irradiance and wind speed, while MT and FC have nonzero minimum output due to dispatch requirements [37]. Ramp-up and ramp-down rates are defined only for dispatchable units (MT and FC) [39], while PV and WT do not require such constraints. The ESS is modeled with a negative minimum power value, indicating its discharge capacity. Additionally, the energy output of PV and WT is bounded above by their resource-based generation potential, and not by demand-based dispatch. Therefore, the maximum power levels for these units represent generation ceilings rather than adjustable dispatch values.

All computational experiments are carried out using the Gurobi solver on a system with an Intel core i9–9900 CPU at 3.60 GHz and 32 GB RAM. The Gurobi solver version 12.0.0 is employed with its default parameter settings. The proposed reformulation-and-decomposition algorithm and all mathematical models are implemented in C#. For the configuration of the reformulation-and-decomposition algorithm, the tolerance ε is set to 10^{-4} .

5.2. Case study on DRP settings

The first computational experiment deals with case studies comparing two different DRP settings for the development of decentralized power grid systems as follows:

(i) Case Study 1: subsidy-only DRP

(ii) Case Study 2: mixed DRPs with RTP and subsidy

In this experiment, Case Study 1 serves as the benchmark scenario. In the formulated bilevel optimization problem, the ISO determines DRP parameters based on the anticipated responses of electricity users. However, due to the hierarchical structure of the problem, bilevel feasibility is not satisfied if the followers' decisions violate the leader's budget constraints. This study explores whether a mixed DRP setting improves the ability to find bilevel feasible solutions and examines its effectiveness in enhancing the ISO's primary objective of grid stabilization. In Case Study 1, the RTP decision variables in the proposed algorithm are fixed at the SMP values provided in Table 1. Consequently, the RMP in Case Study 1, where only the subsidy program is applied, can be formulated as a mixed-integer linear programming (MILP) model through the linearization of discrete bilinear terms $x_k^{\rm sub}y_{ik}$. Conversely,

in Case Study 2, where both RTP and subsidy programs are utilized, the RMP includes continuous bilinear terms $x_i^{\rm rtp} p_{it}^{\rm in}$, resulting in a nonconvex mixed-integer quadratically constrained quadratic programming (MIQCQP) model. This structural difference in the optimization problem highlights the computational complexity associated with integrating RTP into the DRPs.

Table 3 presents the comparative results between Case Study 1 and Case Study 2 for instances with three electricity users. Bold values indicate cases where a bilevel feasible solution was not found, prompting an additional process in which the leader's decision x was fixed at the final solution of RMP, and then SP2 was solved without the budget constraint. Due to the MILP formulation of RMP, Case Study 1 was solved significantly faster than Case Study 2, which involved a nonconvex MIQCOP model. In several instances, Case Study 2 did not converge within the five-hour time limit, as Gurobi attempted to obtain a global optimum. Some instances resulted in infeasibility in both case studies, meaning no bilevel feasible solution could be found. However, for budget levels of 35 and 60, Case Study 2 successfully found bilevel feasible solutions, whereas Case Study 1 did not, suggesting that the RTP mechanism can mitigate violations of the ISO's budget constraint caused by the followers' best responses. However, it is not easy to generalize this finding based on only two instances. In terms of grid cost and peak load minimization, Case Study 2 achieved the lowest overall system cost and peak load compared to Case Study 1. However, this reduction came at the expense of higher follower operational costs, indicating that the mixed DRP setting shifts economic burdens onto electricity users. Additionally, the proposed algorithm for Case Study 2 did not converge within the five-hour limit for certain instances, highlighting the computational challenge of solving a non-convex MIQCQP model due to the bilinear terms introduced by RTP decisions.

5.3. Analysis of grid stabilization and budget usage

Figs. 3 and 4 illustrate the impact of budget allocation on peak load reduction and budget usage in Case Study 1 and Case Study 2, respectively. As the budget increases, peak load decreases significantly in both cases, demonstrating the effectiveness of DRPs in managing demand. In Case Study 1, notable reductions in peak load are observed when the budget is set at 15 and 30, suggesting that these budget levels provide the most cost-effective peak load reduction. However, budget usage is not maximized in all instances, indicating that certain budget allocations

Table 3Comparative results of Case Study 1 and Case Study 2.

B(\$)	Case Study	y 1					Case Study	y 2				
	CPU (min.)	F ₁ (kWh)	F ₂ (\$)	<i>f</i> ₁ (\$)	<i>f</i> ₂ (\$)	f ₃ (\$)	CPU (min.)	F_1 (kWh)	F ₂ (\$)	<i>f</i> ₁ (\$)	<i>f</i> ₂ (\$)	f ₃ (\$)
0	0.0	271.0	0.0	21.5	21.8	22.0	0.4	73.0	0.0	50.6	52.3	51.7
5	0.1	265.0	3.9	21.5	21.8	22.0	0.9	71.4	5.0	52.8	53.9	53.0
10	0.0	259.0	7.9	21.5	21.8	22.0	1.2	71.4	10.0	51.2	52.3	51.4
15	0.0	241.0	14.3	21.5	21.8	22.0	2.2	69.8	15.0	52.6	54.0	53.1
20	0.1	235.0	18.2	21.5	21.8	22.0	19.8	69.8	19.5	51.6	52.4	51.7
25	0.1	229.0	22.2	21.5	21.8	22.0	0.6	68.1	25.0	53.1	54.2	53.3
30	0.1	211.0	28.6	21.5	21.8	22.0	9.5	65.5	30.0	52.2	53.5	52.5
35	0.4	229.0	138.1	21.4	21.7	22.0	43.0	65.5	30.0	51.6	53.0	52.6
40	0.2	199.0	36.5	21.5	21.8	22.0	+5hs	_	_	_	-	_
45	1.0	299.0	108.3	20.9	21.2	21.5	+5hs	_	_	-	-	_
50	0.5	193.0	40.4	21.5	21.8	22.0	24.7	62.2	48.7	52.4	53.8	52.9
55	3.0	186.0	55.0	21.4	21.7	21.9	+5hs	_	_	-	-	_
60	1.8	207.9	231.8	19.7	20.0	20.3	282.2	60.0	60.0	53.0	54.3	53.3
65	1.1	186.0	65.0	18.0	18.3	18.6	30.1	60.0	65.0	51.4	52.7	52.1
70	5.2	211.0	150.8	21.3	21.6	21.9	+5hs	_	-	-	-	-
75	2.5	207.9	153.7	20.4	20.7	20.9	+5hs	_	_	-	-	_
80	7.8	207.9	158.7	18.7	19.0	19.3	+5hs	_	_	-	-	_
85	6.1	211.0	153.3	20.5	20.8	21.1	+5hs	_	_	-	-	_
90	2.9	142.1	154.8	20.2	20.3	20.6	+5hs	_	_	_	_	_
95	4.5	142.1	159.7	18.6	18.7	19.0	+5hs	_	_	_	_	-
100	2.9	137.3	187.0	20.3	20.5	20.7	+5hs	-	-	-	-	-

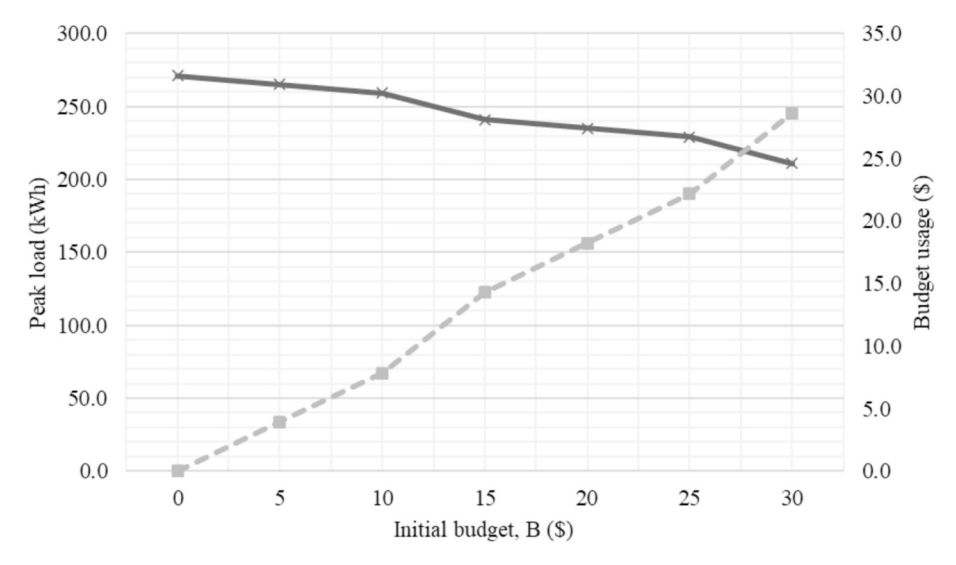


Fig. 3. Peak load reduction and budget usage under Case Study 1.

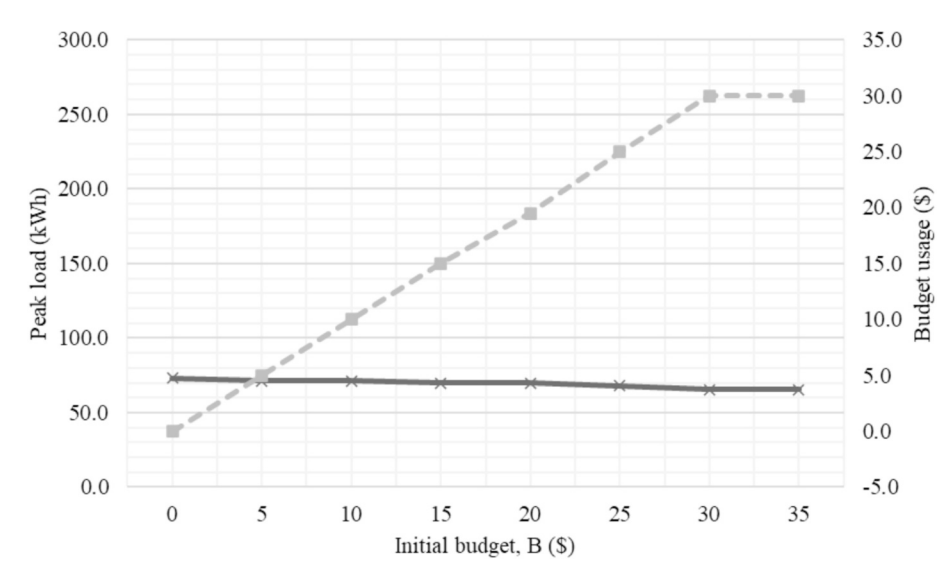


Fig. 4. Peak load reduction and budget usage under Case Study 2.

may not be fully utilized for subsidy distribution. In contrast, Case Study 2 consistently utilizes the allocated budget across most budget settings. Despite this, evaluating the efficiency of budget usage in terms of peak load reduction remains challenging, as the integration of RTP inherently enhances demand-side response. The simultaneous implementation of RTP and subsidies results in a more substantial reduction in peak load compared to the subsidy-only scenario, making direct comparisons of budget efficiency between the two cases non-trivial.

Notably, in Case Study 2, a temporary increase in peak load is observed at certain budget levels (e.g., 35 or 60) despite the application of RTP. This behavior can be attributed to the elasticity-driven concentration of user demand during low-RTP hours, which may inadvertently create new peaks if not offset by sufficient DER activation. When the ISO sets low retail prices for specific time slots to shift demand, some users may concentrate on their consumption within these intervals, leading to secondary peaks. Additionally, limited DER generation capacity or unavailability during those time slots may restrict the system's ability to flatten the load curve effectively. This result highlights a nontrivial effect of dynamic pricing mechanisms: while they improve overall flexibility and reduce average costs, they may also introduce localized fluctuations in peak demand under certain conditions. Such dynamics

suggest that RTP policies must be carefully designed in conjunction with DER planning and load diversity analysis to avoid unintended peak rebounds.

Tables 4 and 5 present the optimal subsidy rates determined by the ISO in Case Study 1 and Case Study 2 under different budget allocations. The values represent the proportion of installation costs covered by subsidies for each DER unit, including costs of the MT, FC, PV, WT, and ESS. In Case Study 1, the allocation of subsidies varies significantly across different DER types. While subsidies for FC and PV increase as the budget rises, MT and WT receive limited or no subsidies under most

Table 4Subsidy rates determined by the ISO under Case Study 1.

Subsidy rate	Initial	budget I	3					
	0	5	10	15	20	25	30	35
$x_{ m MT}^{ m sub}$	0 %	41 %	41 %	0 %	41 %	41 %	0 %	41 %
x_{FC}^{sub}	0 %	23 %	47 %	67 %	67 %	67 %	67 %	67 %
$x_{\mathrm{pV}}^{\mathrm{sub}}$	0 %	0 %	38 %	56 %	75 %	0 %	90 %	90 %
$x_{ m WT}^{ m sub}$	0 %	44 %	87 %	0 %	0 %	0 %	0 %	0 %
$x_{\rm ESS}^{ m sub}$	0 %	0 %	30 %	45 %	60 %	75 %	90 %	95 %

Table 5Subsidy rates determined by the ISO under Case Study 2.

Subsidy rate	Initial	budget B						
	0	5	10	15	20	25	30	35
$x_{ m MT}^{ m sub}$	0 %	0 %	0 %	0 %	0 %	0 %	0 %	0 %
x_{FC}^{sub}	0 %	0 %	1 %	0 %	0 %	0 %	0 %	1 %
$x_{ m PV}^{ m sub}$	0 %	0 %	0 %	0 %	0 %	0 %	0 %	0 %
$x_{ m WT}^{ m sub}$	0 %	77 %	80 %	76 %	78 %	76 %	0 %	0 %
$x_{\rm ESS}^{ m sub}$	92 %	96 %	95 %	96 %	96 %	96 %	95 %	96 %

budget levels. An ESS begins receiving subsidies only when the budget exceeds 10, with the subsidy rate reaching 95 % at the highest budget level. In contrast, Case Study 2 exhibits a different subsidy distribution pattern due to the presence of RTP. The ISO consistently prioritizes subsidizing the ESS across all budget levels, maintaining a subsidy rate of approximately 95 %, regardless of budget size. The WT also receives relatively high levels of subsidy, particularly when the budget ranges from 5 to 20, with values exceeding 75 %. However, for higher budgets (30 and 35), the subsidy rate for WT drops to zero, indicating a shift in prioritization. Meanwhile, the MT and PV consistently receive no subsidy, and FC only receives marginal support at limited budget levels. These results suggest that the RTP mechanism influences the ISO's strategy by concentrating subsidies on storage and, to some extent, renewables like WT under certain conditions, while reducing support for dispatchable or high-cost generation units.

These results highlight how the introduction of RTP influences the ISO's subsidy allocation strategy. The ISO in Case Study 2 allocates subsidies predominantly to ESS and renewable generation, whereas in Case Study 1, a more varied subsidy distribution is observed. This suggests that RTP not only impacts electricity pricing but also affects investment decisions related to DER deployment.

Table 6 presents the RTP decisions made by the ISO under Case Study 2 across different initial budget levels. The values in the table represent the electricity price determined by the ISO for each hour in a twenty-four-hour period, considering varying budget constraints. Several key observations can be made from the results. First, for budget levels of 0 and 5, the RTP remains close to the predefined lower bound in most hours, indicating that the ISO has limited flexibility in adjusting prices

Table 6
RTP decisions made by the ISO under Case Study 2 (¢/kWh).

Time	Initial	budget B						
	0	5	10	15	20	25	30	35
0	0.52	0.52	0.24	0.52	0.52	0.52	0.24	0.52
1	0.52	0.52	0.24	0.52	0.52	0.52	0.24	0.52
2	0.52	0.52	0.39	0.52	0.52	0.52	0.24	0.52
3	0.52	0.69	0.52	0.52	0.69	0.52	0.52	0.52
4	0.52	0.52	0.52	0.52	0.52	0.52	0.52	0.52
5	0.52	0.52	0.52	0.52	0.52	0.52	0.52	0.52
6	6.00	5.99	4.61	6.00	0.52	6.00	6.00	4.82
7	0.52	5.99	3.70	6.00	6.00	6.00	6.00	6.00
8	1.50	5.99	4.61	6.00	6.00	6.00	6.00	6.00
9	6.00	5.99	4.61	6.00	4.82	6.00	6.00	6.00
10	6.00	5.99	4.61	6.00	6.00	6.00	6.00	6.00
11	6.00	4.82	4.61	6.00	6.00	6.00	4.82	6.00
12	6.00	5.99	4.82	6.00	4.82	6.00	4.82	6.00
13	6.00	5.99	6.00	4.82	4.82	6.00	5.75	6.00
14	2.00	5.99	4.82	6.00	6.00	6.00	4.82	4.82
15	6.00	5.99	6.00	6.00	4.82	6.00	6.00	6.00
16	6.00	5.99	6.00	6.00	6.00	6.00	6.00	6.00
17	6.00	5.99	6.00	6.00	6.00	6.00	6.00	6.00
18	6.00	5.99	6.00	6.00	6.00	6.00	6.00	6.00
19	6.00	5.99	6.00	6.00	4.82	6.00	6.00	6.00
20	6.00	5.99	6.00	6.00	6.00	6.00	6.00	6.00
21	6.00	4.82	6.00	6.00	6.00	6.00	6.00	0.54
22	0.52	5.99	6.00	0.52	6.00	6.00	0.52	0.52
23	0.52	0.52	0.52	0.52	0.52	0.52	0.52	0.52

due to financial constraints. As the budget increases, the ISO actively utilizes higher RTP values, particularly during peak demand hours (e.g., 6 a.m. to 8 p.m.), suggesting a strategic pricing adjustment to manage grid stability. Notably, when the budget reaches 10 or higher, the RTP values begin fluctuating more dynamically, reflecting the ISO's ability to fine-tune pricing mechanisms to influence electricity consumption patterns effectively. Another critical trend is that the RTP consistently reaches the predefined upper bound (six cents/kWh) during high-demand periods, indicating that the ISO fully exploits its pricing flexibility under larger budget allocations. This pricing strategy aligns with the objective of peak load reduction by encouraging users to shift consumption to lower-priced periods. However, during low-demand hours (e.g., early morning and late night), RTP values remain near the lower bound, minimizing unnecessary price surges while maintaining economic efficiency.

These findings highlight the role of RTP in demand-side management under a mixed DRP setting. The results indicate that increasing the budget allows the ISO to exert greater control over electricity pricing, thereby optimizing demand response effectiveness and improving grid stability.

To complement the analysis of Table 6 and to clarify the behavioral and cost implications of RTP, we provide additional visual and numerical comparisons. Fig. 5 presents the hourly profiles of SMP and RTP under a budget level of 20. While SMP remains relatively low and stable throughout the day, RTP increases sharply during the daytime hours from 8:00 to 20:00. This indicates that the ISO uses time-varying prices to reduce demand during peak periods. The gap between SMP and RTP represents the economic signal intended to guide user behavior.

Tables 7 and 8 present a side-by-side comparison of user-level outcomes under two different demand response settings: one based on subsidies only (Case Study 1), and the other combining RTP with targeted subsidies (Case Study 2). In the subsidy-only case, users 1 and 2 adopt MT and FC, receiving subsidy rates of 41 % and 67 %, respectively. These units generate significant amounts of electricity—408 kW-hours and 531 kW-hours for User 1—but User 1 still purchases 704 kW-hours from the grid, resulting in a daily purchase cost of 5.43 dollars. Users 2 and 3, who follow similar installation decisions, purchase 1706 kW-hours and 1670 kW-hours, incurring costs of 21.76 and 22.03 dollars per day.

In Case Study 2, users respond differently under the influence of RTP. User 1 adds a WT, which receives a 78 % subsidy, reducing its net cost to 2.61 dollars. The user's generation increases accordingly, while electricity purchased from the grid falls to 280.12 kW-hours. However, the daily purchase cost rises to 13.32 dollars, reflecting the higher RTP during certain hours. User 2 adds both WT and an ESS, receiving subsidies of 78 % and 96 %, respectively. With these additions, User 2 reduces grid purchases to 275.35 kW-hours and lowers the purchase cost to 12.28 dollars. The ESS actively contributes to cost control, charging 43.75 kW-hours and discharging 35.44 kW-hours. Although User 3 maintains the same DER installation in both cases, the daily purchase cost increases from 22.03 to 26.25 dollars under RTP, despite a reduction in purchased electricity. This is due to the user's exposure to elevated RTP levels during peak periods.

Overall, these results show that users with flexible resources such as ESS and WT can respond more effectively to RTP, both in terms of reducing grid dependence and in managing daily costs. In contrast, users without such flexibility may face higher expenses even when their total electricity purchases are reduced. These findings highlight the importance of aligning pricing signals with user capability and DER availability, especially when RTP is used to support demand-side coordination under limited budgets.

5.4. Performance tests

Table 9 presents the computational performance of the proposed reformulation-and-decomposition algorithm under varying budget

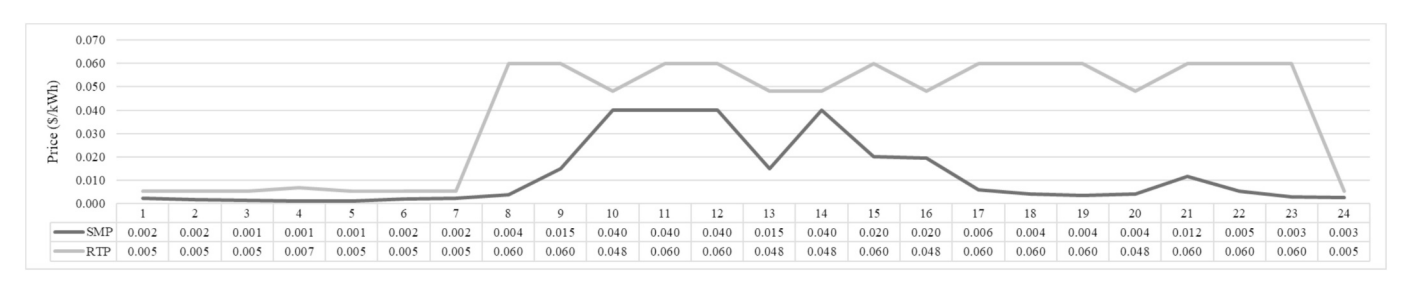


Fig. 5. SMP vs RTP over Time (Budget = 20).

levels. The table aggregates experimental results across different numbers of electricity users (one to three) and reports the average values for key performance indicators. The columns include the initial budget B, the average total CPU time required to solve the problem, the number of RMP steps, the average CPU time per RMP iteration, the number of successful SP2 solutions, the number of infeasible SP2 instances, and the average CPU time for solving SP2. The results indicate that computational performance varies significantly with the allocated budget. Notably, at B = 10, the total CPU time is substantially higher than it is when compared to solving times required for other budget levels, suggesting that the algorithm encounters more complex bilevel interactions that require additional iterations for convergence. The number of RMP steps increases with budget, particularly beyond B = 20, which implies that larger budgets allow the ISO to explore more complex DRP settings before convergence. Similarly, the number of SP2 infeasibilities tends to rise with budget, highlighting the challenge of ensuring bilevel feasibility as the leader's DRP decisions become more intricate.

Table 10 summarizes the computational performance of the proposed algorithm under different numbers of electricity users. The reported values are averaged over all budget settings to analyze how the number of users affects computational complexity. The columns provide the average total CPU time, the number of RMP steps, the average CPU time per RMP iteration, the number of successful SP2 solutions, the number of infeasible SP2 instances, and the average CPU time for solving SP2. The findings reveal that as the number of users increases, the computational burden of the algorithm grows significantly. When the number of users increases from 1 to 3, the total CPU time exhibits a sharp increase, indicating the increased complexity of solving bilevel optimization problems with multiple followers. The number of RMP steps and SP2 infeasibilities also increase, confirming that larger user groups lead to more complex interactions that require additional iterations for convergence. However, despite the increased computational complexity, the proposed algorithm successfully identifies feasible solutions in most budget settings, demonstrating its robustness in handling multi-follower bilevel optimization problems.

It should also be noted that the experimental setup assumes a homogeneous user base with normally distributed demand profiles. While this assumption facilitates tractable computation and controlled validation of the proposed bilevel structure, it may not fully capture the diversity of user behaviors in real-world power systems. The current setting was designed primarily to isolate and evaluate the structural performance of the algorithm under exact bilevel modeling. Future studies will aim to extend the model by incorporating clustered user groups and empirical load data from residential, commercial, and industrial sectors to enhance behavioral realism and scalability assessment.

Although the results reveal scalability limitations, particularly in instances involving more than two users, the proposed algorithm retains significant value as a benchmark tool for future method development. Despite the increase in computational time with user count, it provides exact solutions for small- to medium-scale bilevel instances that include both discrete user decisions and bilinear leader-follower interactions. While the current formulation does not enable practical solution times

for large-scale systems, it establishes a foundational basis for evaluating the performance of heuristic and approximation-based approaches. Future bilevel methods aiming for scalability may benefit from using this algorithm as a reference to assess optimality gaps, generate high-quality initial solutions, or derive primal-dual bounds in complex grid decision environments

5.5. Managerial insights

The findings reveal key trade-offs between grid stability, financial feasibility, and computational efficiency. In particular, combining RTP with subsidy programs improves the likelihood of bilevel feasibility, especially in scenarios involving diverse user behaviors and constrained budgets. In contrast, subsidy-only programs often result in budget violations due to their limited flexibility in guiding user behavior. The results suggest that RTP provides a complementary mechanism for managing demand-side decisions, helping the ISO accommodate diverse user responses while staying within budget. This effect was especially evident in certain budget scenarios, where the mixed DRP approach successfully prevented infeasibilities that occurred under subsidy-only settings.

From a computational perspective, the results reveal notable challenges in solving bilevel optimization problems involving mixed DRP settings. The non-convex MIQCQP structure of Case Study 2 led to significantly longer computational times, with some instances failing to converge within the solver's time limit. This increased complexity highlights a fundamental trade-off: while mixed DRP settings enhance feasibility and grid stability, they introduce additional computational burdens. These results emphasize the need for computationally efficient algorithms, especially as the number of participants and decision variables increases. Research into scalable reformulation techniques or learning-based approximations could further reduce solution times without compromising optimality. These findings suggest that a hybrid scheme may support both DER adoption and behavioral flexibility, particularly in contexts where static incentives alone are insufficient. For example, tiered pricing schemes or time-of-use incentives aligned with DER performance metrics could improve load diversity and grid reliability.

The study also carries important policy implications for managing decentralized power grids. The subsidy mechanism is effective in incentivizing DER adoption, which contributes to long-term sustainability by increasing renewable energy integration. However, the results indicate that without an RTP component, users may not optimally adjust their electricity consumption, potentially leading to inefficient grid operations. A hybrid DRP structure that combines both financial incentives and market-driven pricing strategies is recommended to improve demand-side management. Additionally, differentiated pricing models based on user profiles and DER adoption status could enhance the effectiveness of DRPs. By considering these strategic elements, policymakers can design more adaptive and resilient power grid systems.

Overall, the findings of this study reinforce the value of mixed DRP settings in decentralized power grid management. While subsidy programs alone can drive DER adoption, the integration of RTP provides

 Table 7

 DER adoption, electricity use, and cost outcomes under Case Study 1.

DEN auopt.	ייייי, כוכר	uicity use, o	and cost on	comes miner	DEN auopinon, electricity use, and cost outcomes miner case study 1.										
Follower	DERs	Follower DERs Capital Subsidy Cost Rate	Subsidy Rate	Subsidy Amount	Maintenance Cost	Operating Cost	Net Cost	Power Generated	Power Charged	Power Discharged	Cost per kWh of Daily Generation	Electricity Purchased (kWh)	Electricity Sold to ISO (kWh)	Electricity Purchase Cost (\$/day)	Electricity Sales Revenue (\$/day)
User 1		(6		,	0	6			6	704.00	0.00	5.43	0
	MT	9.58	41 %	3.93		1.64	7.29	408.00			0.02				
	FC	21.29	% 29	14.31		1.07	8.04	531.00			0.02				
User 2												1706.00	0.00	21.76	0
User 3												1670.00	0.00	22.03	0

 Table 8

 DER adoption, electricity use, and cost outcomes under Case Stud

DER adopt	ion, elec	tricity use,	and cost on	tcomes unde	DER adoption, electricity use, and cost outcomes under Case Study 2.										
Follower	Follower DERs Capital	Capital	Subsidy	Subsidy	Maintenance	Operating	Net	Power	Power	Power	Cost per kWh of		Electricity	Electricity	Electricity
		Cost	Rate	Amount	Cost	Cost	Cost	Generated	Charged	Discharged	Daily	Purchased	Sold to ISO	Purchase Cost	Sales
											Generation	(kWh)	(kWh)	(\$/day)	Revenue (\$/day)
User 1												280.12	0.00	13.32	0
	MT	9.58	% 0	0.00		2.35	11.93	585.73			0.02				
	FC	21.29	% 0	0.00		1.45	22.74	720.00			0.03				
	WT	11.44	% 82	8.89	90.0		2.61	57.15			0.05				
User 2												275.35	0.00	12.28	0
	MT	9.58	% 0	0.00		2.66	12.24	661.82			0.02				
	FC	21.29	% 0	0.00		1.45	22.74	720.00			0.03				
	MT	11.44	% 82	8.89	90.0		2.61	57.15			0.05				
	ESS	33.20	% 96	31.77			1.43		43.75	35.44					
User 3												396.00	0.00	16.25	0
	MT	9.58	% 0	0.00		0.00	9.58	554.00			0.02				
	FC	21.29	% 0	0.00		1.45	22.74	720.00			0.03				

Table 9Computational performance of the proposed algorithm under varying initial budget levels.

B(\$)	Avg. Total CPU	RMP		SP2		
		No. of Steps	Avg. CPU	No. of solved	No. of infeasible	Avg. CPU
0	1.0	2.0	0.2	2.0	0.0	0.3
5	2.4	4.0	0.2	2.2	1.8	0.4
10	929.7	14.0	45.7	6.2	7.8	0.1
15	1.4	3.0	0.2	2.2	0.8	0.3
20	4.2	7.2	0.3	3.2	4.0	0.3
25	4.1	6.2	0.3	3.8	2.4	0.3
30	5.7	8.0	0.4	4.4	3.6	0.4
35	6.5	10.0	0.4	4.2	5.8	0.2

Table 10Computational performance of the proposed algorithm under different numbers of electricity users.

No. of Users	Avg. CPU	RMP		SP2		
		No. of Steps	Avg. CPU	No. of solved	No. of infeasible	Avg. CPU
1	0.3	5.7	0.1	5.7	0.0	0.0
2	19.4	12.6	1.2	4.9	7.7	0.1
3	37.7	12.8	2.9	3.8	9.0	0.2

greater flexibility in aligning electricity user behavior with grid stability objectives. The proposed algorithm demonstrates strong potential for integration into pilot-scale grid platforms where heterogeneous DER participation is a design priority. Further work may also consider embedding the algorithm into ISO planning tools for daily operational scheduling.

Compared to conventional demand response programs that rely solely on fixed installation subsidies, the proposed mixed incentive mechanism that combines RTP with budget-limited subsidies offers notable advantages in terms of efficiency and adaptability. The simulation results indicate that this approach induces more differentiated user responses and improves system-level outcomes, particularly when users have diverse installation costs or consumption behaviors. RTP provides dynamic economic signals that encourage flexible behavior, while targeted subsidies help lower financial barriers to DER adoption. However, the variability of price signals may introduce behavioral uncertainty for some users, potentially affecting participation stability if not supported by appropriate communication or guidance. This mixed approach is particularly advantageous in contexts marked by high user diversity and policy-driven DER targets. Conversely, in environments requiring stable, predictable program structures, fixed subsidy models may offer more practical benefits despite their lower responsiveness.

6. Conclusion

This study presented a bilevel optimization framework to model the interactions between an ISO and multiple electricity users in a decentralized power grid system. The proposed framework incorporates two key DRPs of RTP and a subsidy mechanism, which together influence user decisions on electricity consumption and DER adoption. To address the inherent computational challenges of bilevel optimization, a reformulation-and-decomposition algorithm was developed, ensuring bilevel feasibility while maintaining computational tractability.

Through computational experiments, two DRP settings were analyzed: (i) a subsidy-only program and (ii) a mixed DRP setting combining RTP and subsidies. The results demonstrated that integrating RTP with subsidies increases the likelihood of finding bilevel feasible solutions by dynamically adjusting electricity prices to influence user responses. Additionally, the mixed DRP setting resulted in more

effective peak load reductions and improved grid stability compared to the subsidy-only program. However, it also introduced additional computational complexity due to the non-convex nature of the optimization problem. These findings highlight the trade-offs between feasibility, grid stability, and computational efficiency in bilevel decision-making processes.

This study has certain limitations that warrant further investigation. The computational experiments were conducted on a finite set of test instances with specific parameter values, meaning that broader generalization requires additional validation on larger-scale power grid models. Furthermore, the problem was analyzed within a single-day operational horizon, whereas real-world grid management often requires multi-period decision-making. Future studies should consider multi-period bilevel optimization models that account for investment decisions over extended planning horizons. Additionally, the development of more advanced decomposition algorithms tailored to nonconvex bilevel models could further enhance solution scalability and computational efficiency.

While large-scale extensions remain computationally intensive, the current approach establishes a strong foundation, and the proposed method offers a rigorous benchmark for future algorithmic developments. In particular, it provides a reliable reference point for evaluating the performance and optimality of metaheuristic or learning-based approaches aimed at solving large-scale bilevel problems that involve both discrete follower decisions and bilinear interactions. The exact solutions obtained from our framework can serve not only as ground-truth baselines for small instances but also as a source of primal-dual bounds or initial solutions in hybrid methods.

Overall, this research underscores the importance of integrating multiple DRP mechanisms to achieve both economic and operational efficiency in decentralized power grid management. The proposed algorithm provides a practical approach to handling bilevel feasibility constraints, enabling more adaptive and resilient grid operations. Future research should continue refining bilevel optimization techniques to address computational challenges and to enhance the applicability of DRP strategies in real-world energy systems.

CRediT authorship contribution statement

Young-Bin Woo: Writing – original draft, Software, Investigation, Conceptualization, Writing – review & editing, Visualization, Methodology, Data curation. **Ilkyeong Moon:** Validation, Conceptualization, Writing – review & editing, Supervision.

Declaration of competing interest

The authors declare that they have no known competing financial interests or personal relationships that could have appeared to influence the work reported in this paper.

Acknowledgements

The authors are grateful for the valuable comments from the area editor and two anonymous reviewers. This work was supported by the National Research Foundation of Korea (NRF) grants funded by the Korean government (Ministry of Science and ICT) [Grant Nos. RS-2023-00218913 and RS-2024-00337285].

Data availability

Data will be made available on request.

References

- [1] Jiang Q, Xue M, Geng G. Energy management of microgrid in grid-connected and stand-alone modes. IEEE Trans Power Syst 2013;28:3380–9. https://doi.org/ 10.1109/TPWRS.2013.2244104.
- [2] Lopes JAP, Madureira A, Gil N, Resende F. Operation of multi-microgrids Microgrids 2013:165–205.
- [3] Ou TC, Hong CM. Dynamic operation and control of microgrid hybrid power systems. Energy 2014;66:314–23. https://doi.org/10.1016/j.energy.2014.01.042.
- [4] Deihimi A, Keshavarz Zahed B, Iravani R. An interactive operation management of a micro-grid with multiple distributed generations using multi-objective uniform water cycle algorithm. Energy 2016;106:482–509. https://doi.org/10.1016/j. energy.2016.03.048.
- [5] Hirsch A, Parag Y, Guerrero J. Microgrids: a review of technologies, key drivers, and outstanding issues. Renew Sustain Energy Rev 2018;90:402–11. https://doi. org/10.1016/j.rser.2018.03.040.
- [6] Haider HT, See OH, Elmenreich W. A review of residential demand response of smart grid. Renew Sustain Energy Rev 2016;59:166–78. https://doi.org/10.1016/j. rser.2016.01.016.
- [7] Basit MA, Dilshad S, Badar R, Sami ur Rehman SM. Limitations, challenges, and solution approaches in grid-connected renewable energy systems. Int J Energy Res 2020;44:4132–62. https://doi.org/10.1002/er.5033.
- [8] Ou TC. A novel unsymmetrical faults analysis for microgrid distribution systems. International Journal of Electrical Power and Energy Systems 2012;43:1017–24. https://doi.org/10.1016/j.ijepes.2012.05.012.
- https://doi.org/10.1016/j.ijepes.2012.05.012.

 [9] Bahramara S, Moghaddam MP, Haghifam MR. Modelling hierarchical decision making framework for operation of active distribution grids. IET Generation, Transmission and Distribution 2015;9:2555–64. https://doi.org/10.1049/ietgtd.2015.0327.
- [10] Marvasti AK, Fu Y, Dormohammadi S, Rais-Rohani M. Optimal operation of active distribution grids: a system of systems framework. IEEE Trans Smart Grid 2014;5: 1228–37. https://doi.org/10.1109/TSG.2013.2282867.
- [11] Rider MJ, López-Lezama JM, Contreras J, Padilha-Feltrin A. Bilevel approach for optimal location and contract pricing of distributed generation in radial distribution systems using mixed-integer linear programming. IET Generation, Transmission and Distribution 2013;7:724–34. https://doi.org/10.1049/ietgtd.2012.0369.
- [12] Sadeghi Mobarakeh A, Rajabi-Ghahnavieh A, Haghighat H. A bi-level approach for optimal contract pricing of independent dispatchable DG units in distribution networks. International Transactions on Electrical Energy Systems 2016;26: 1685–704. https://doi.org/10.1002/etep.2172.
- [13] Liu Y, Guo L, Wang C. A robust operation-based scheduling optimization for smart distribution networks with multi-microgrids. Appl Energy 2018;228:130–40. https://doi.org/10.1016/j.apenergy.2018.04.087.
- [14] Asimakopoulou GE, Dimeas AL, Hatziargyriou ND. Leader-follower strategies for energy management of multi-microgrids. IEEE Trans Smart Grid 2013;4:1909–16. https://doi.org/10.1109/TSG.2013.2256941.
- [15] Wang Y, Mao S, Nelms RM. On hierarchical power scheduling for the macrogrid and cooperative microgrids. IEEE Trans Industr Inform 2015;11:1574–84. https://doi.org/10.1109/TII.2015.2417496.
- [16] Karimi H, Jadid S. Optimal energy management for multi-microgrid considering demand response programs: a stochastic multi-objective framework. Energy 2020; 195:116992. https://doi.org/10.1016/j.energy.2020.116992.
- [17] Li Q, Gao M, Lin H, Chen Z, Chen M. MAS-based distributed control method for multi-microgrids with high-penetration renewable energy. Energy 2019;171: 284–95. https://doi.org/10.1016/j.energy.2018.12.167.
- [18] Radhakrishnan BM, Srinivasan D. A multi-agent based distributed energy management scheme for smart grid applications. Energy 2016;103:192–204. https://doi.org/10.1016/j.energy.2016.02.117.
- [19] Nikmehr N, Najafi Ravadanegh S. Optimal power dispatch of multi-microgrids at future smart distribution grids. IEEE Trans Smart Grid 2015;6:1648–57. https:// doi.org/10.1109/TSG.2015.2396992.
- [20] Feijoo F, Das TK. Emissions control via carbon policies and microgrid generation: a bilevel model and Pareto analysis. Energy 2015;90:1545–55. https://doi.org/ 10.1016/j.energy.2015.06.110.

- [21] Han D, Lee JH. Two-stage stochastic programming formulation for optimal design and operation of multi-microgrid system using data-based modeling of renewable energy sources. Appl Energy 2021;291:116830. https://doi.org/10.1016/j. apenergy.2021.116830.
- [22] Haddadian H. Noroozian R. Erratum to "Multi-microgrids approach for design and operation of future distribution networks based on novel technical indices" [Appl. Energy 185 (2017) 650–663] (Applied Energy, (80306261916315690), (10.1016/j.apenergy.2016.10.120)). Appl Energy 2017;202:783. https://doi.org/10.1016/j.apenergy.2017.06.102.
- [23] Gregoratti D, Matamoros J. Distributed energy trading: the multiple-microgrid case. IEEE Trans Ind Electron 2015;62:2551–9. https://doi.org/10.1109/ TIE 2014 2352592.
- [24] Mengelkamp E, Gärttner J, Rock K, Kessler S, Orsini L, Weinhardt C. Designing microgrid energy markets: a case study: the Brooklyn microgrid. Appl Energy 2018;210:870–80. https://doi.org/10.1016/j.apenergy.2017.06.054.
- [25] Saad W, Han Z, Poor HV. Coalitional game theory for cooperative micro-grid distribution networks. IEEE International Conference on Communications 2011: 1–5. https://doi.org/10.1109/iccw.2011.5963577.
- [26] Wang Z, Yu X, Mu Y, Jia H. A distributed peer-to-peer energy transaction method for diversified prosumers in Urban Community microgrid system. Appl Energy 2020;260:114327. https://doi.org/10.1016/j.apenergy.2019.114327.
- [27] Ren Y, Suganthan PN, Srikanth N. Ensemble methods for wind and solar power forecasting - a state-of-the-art review. Renew Sustain Energy Rev 2015;50:82–91. https://doi.org/10.1016/j.rser.2015.04.081.
- [28] Izadbakhsh M, Gandomkar M, Rezvani A, Ahmadi A. Short-term resource scheduling of a renewable energy based micro grid. Renew Energy 2015;75: 598–606. https://doi.org/10.1016/j.renene.2014.10.043.
- [29] Arefifar SA, Mohamed YARI, El-Fouly THM. Supply-adequacy-based optimal construction of microgrids in smart distribution systems. IEEE Trans Smart Grid 2012;3:1491–502. https://doi.org/10.1109/TSG.2012.2198246.
- [30] Hong CM, Ou TC, Lu KH. Development of intelligent MPPT (maximum power point tracking) control for a grid-connected hybrid power generation system. Energy 2013;50:270–9. https://doi.org/10.1016/j.energy.2012.12.017.
- [31] Kovács A. Bilevel programming approach to demand response management with day-ahead tariff. Journal of Modern Power Systems and Clean Energy 2019;7: 1632–43. https://doi.org/10.1007/s40565-019-0569-7.
- [32] Lu J, Shi C, Zhang G, Dillon T. Model and extended Kuhn-Tucker approach for bilevel multi-follower decision making in a referential-uncooperative situation. Journal of Global Optimization 2007;38:597–608. https://doi.org/10.1007/ s10898-006-9098-9.
- [33] Yue D, Gao J, Zeng B, You F. A projection-based reformulation and decomposition algorithm for global optimization of a class of mixed integer bilevel linear programs. Journal of Global Optimization 2019;73:27–57. https://doi.org/ 10.1007/s10898-018-0679-1.
- [34] Zeng B, An Y. Solving Bilevel mixed integer program by reformulations and decomposition. Optimization Online 2014:1–34.
- [35] Jalali M, Zare K, Seyedi H. Strategic decision-making of distribution network operator with multi-microgrids considering demand response program. Energy 2017;141:1059-71. https://doi.org/10.1016/j.energy.2017.09.145
- 2017;141:1059–71. https://doi.org/10.1016/j.energy.2017.09.145.
 [36] Kazempour SJ, Conejo AJ, Ruiz C. Strategic generation investment using a complementarity approach. IEEE Trans Power Syst 2011;26:940–8. https://doi.org/10.1109/TPWRS.2010.2069573.
- [37] Rana MJ, Zaman F, Ray T, Sarker R. Heuristic enhanced evolutionary algorithm for community microgrid scheduling. IEEE Access 2020;8:76500–15. https://doi.org/ 10.1109/ACCESS.2020.2989795.
- [38] Qi J, Lai C, Xu B, Sun Y, Leung KS. Collaborative energy management optimization toward a green energy local area network. IEEE Trans Industr Inform 2018;14: 5410–8. https://doi.org/10.1109/TII.2018.2796021.
- [39] Sufyan M, Rahim NA, Tan CK, Muhammad MA, Raihan SRS. Optimal sizing and energy scheduling of isolated microgrid considering the battery lifetime degradation. PloS One 2019;14:1–28. https://doi.org/10.1371/journal. pone 0211642
- [40] Logenthiran T, Srinivasan D, Khambadkone AM, Raj TS. Optimal sizing of an islanded microgrid using Evolutionary Strategy. 2010 IEEE 11th international conference on probabilistic methods applied to power systems. PMAPS 2010;2010: 12–7. https://doi.org/10.1109/PMAPS.2010.5528840.